© 2019. Published by The Company of Biologists Ltd | Journal of Cell Science (2019) 132, jcs233130. doi:10.1242/jcs.233130

RESEARCH ARTICLE

A direct interaction between survivin and myosin II is required for cytokinesis

Aryeh Babkoff, Einav Cohen-Kfir, Hananel Aharon, Daniel Ronen*, Michael Rosenberg‡, Reuven Wiener and Shoshana Ravid§

ABSTRACT

An acto-myosin contractile ring, which forms after anaphase onset and is highly regulated in time and space, mediates cytokinesis, the final step of mitosis. The chromosomal passenger complex (CPC), composed of Aurora-B kinase, INCENP, borealin and survivin (also known as BIRC5), regulates various processes during mitosis, including cytokinesis. It is not understood, however, how CPC regulates cytokinesis. We show that survivin binds to non-muscle myosin II (NMII), regulating its filament assembly. Survivin and NMII interact mainly in telophase, and Cdk1 regulates their interaction in a mitotic-phase-specific manner, revealing the mechanism for the specific timing of survivin–NMII interaction during mitosis. The survivin–NMII interaction is indispensable for cytokinesis, and its disruption leads to multiple mitotic defects. We further show that only the survivin homodimer binds to NMII, attesting to the biological importance for survivin homodimerization. We suggest a novel function for survivin in regulating the spatio-temporal formation of the acto-NMII contractile ring during cytokinesis and we elucidate the role of Cdk1 in regulating this process.

This article has an associated First Person interview with the first author of the paper.

KEY WORDS: Cytokinesis, Non-muscle myosin II, Survivin

INTRODUCTION

The aim of mitosis is to separate the genome during cell division and ensure that the two daughter cells inherit an equal and identical complement of chromosomes (Wieser and Pines, 2015). To achieve this, eukaryotic cells completely reorganize their microtubules to build a mitotic spindle that pulls apart the sister chromatids, and subsequently reorganize the acto-myosin cytoskeleton to divide the cell into two and achieve cytokinesis (D'Avino et al., 2015). Cytokinesis requires the assembly and constriction of an equatorial contractile ring composed of F-actin, non-muscle myosin II (NMII) and other cytoskeletal components. The NMII molecule is composed of two heavy chains and two pairs of light chains (Fig. 1A). The heavy chains consist of an N-terminal motor domain containing the actin-binding and ATPase activity, and a tail domain (Vicente-Manzanares et al., 2009). The tail domain is responsible for the assembly of NMII monomers into filaments, which are the functional structures required for NMII activity (Dulyaninova et al., 2005; Murakami et al., 2000; Ronen and Ravid, 2009; Rosenberg and Ravid, 2006). Studies in multiple systems indicate that the targeting signals for cleavage-furrow localization reside in the tail of NMII (Beach and Egelhoff, 2009; Lister et al., 2006; Motegi et al., 2004; Ronen and Ravid, 2009; Sabry et al., 1997). NMII is dispersed throughout the cytoplasm until telophase, when it concentrates in the cortex, especially around the equator, where the furrow forms (Robinson et al., 2002; Vale et al., 2009). Signals from the mitotic spindle and cell cycle machinery control the position of the contractile ring and the timing of its constriction. Centralspindlin is essential for positioning the contractile ring (Carmena et al., 2012). Centralspindlin is a heterotetramer of a dimeric kinesin-6 motor and a dimeric Rho family GTPase-activating protein, and it binds the Rho-GEF Ect-2, the pivotal activator of the small GTPase RhoA (Nishimura and Yonemura, 2006; Yüce et al., 2005). RhoA controls the assembly and constriction of the contractile ring by activating Rho-associated kinase (ROCK, herein referring to both ROCK1 and ROCK2), which increases myosin light chain phosphorylation, promoting NMII contractility (Matsumura et al., 2011). Because the contractile ring is confined to a narrow band of cortex around the equator, it forms a cleavage furrow that drives the ingression of the plasma membrane at the division site during cytokinesis (Robinson et al., 2002; Vale et al., 2009).

The chromosomal passenger complex (CPC) is a protein complex composed of Aurora B kinase, inner centromeric protein (INCENP), borealin and survivin (also known as BIRC5) (Carmena et al., 2012). The CPC plays a crucial role in mitosis, including cytokinesis. The site of the contractile ring assembly and the timing of its constriction are closely coordinated with chromosome segregation, to allow accurate partitioning of the genome and the formation of the two daughter cells. The CPC plays an important role in coordinating and regulating these processes through its functions in central spindle formation, regulation of furrow ingression and abscission (Carmena et al., 2012). The CPC must be released from the chromosomes and targeted to the central spindle for successful cytokinesis. This release requires the interaction of INCENP and Aurora B with the mitotic kinesin-like protein 2 (Mklp2, also known as KIF20A) (Hill et al., 2000; Kitagawa et al., 2013). Mklp2–Aurora B localization to the equatorial cortex, is accomplished by at least in part by the binding of Mklp2 to NMII and actomyosin filaments (Kitagawa et al., 2013). This recruitment event is also required to promote the accumulation of active RhoA at the equatorial cortex and stable ingression of the cleavage furrow (Kitagawa et al., 2013).

Survivin is essential for targeting the CPC to the centromere during mitosis (Kelly et al., 2010; Wang et al., 2010; Yamagishi

Department of Biochemistry and Molecular Biology, The Institute of Medical Research Israel-Canada, The Hebrew University-Hadassah Medical School, Jerusalem 91120, Israel.
*Present address: Hadassah Medical Center, Jerusalem 91120, Israel. ‡Present address: Department of Genetics, Harvard Medical School, Boston, MA 02114, USA.

§Author for correspondence (shoshr@ekmd.huji.ac.il)

S.R., 0000-0001-8017-3259

Received 10 April 2019; Accepted 14 June 2019

Journal of Cell Science (2019) 132, jcs233130. doi:10.1242/jcs.233130

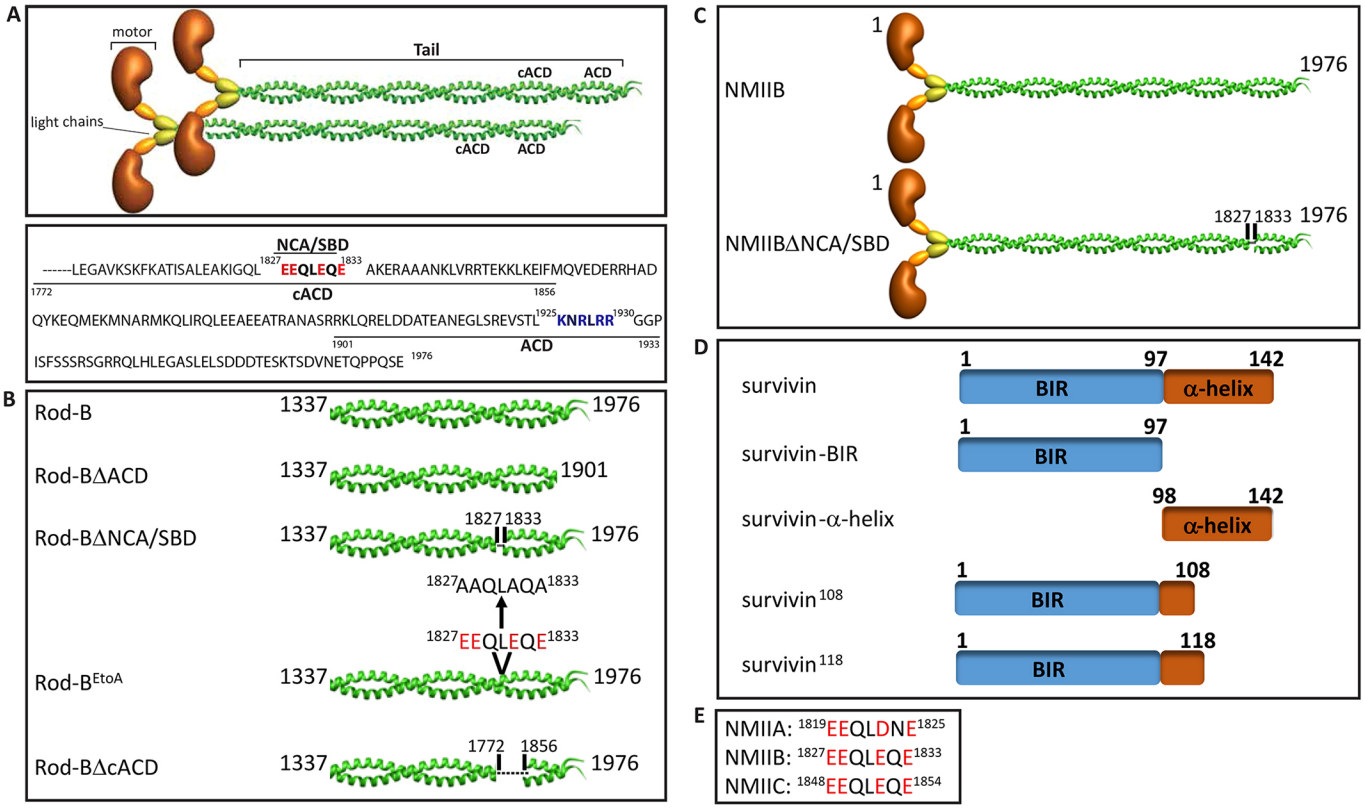

Fig. 1. NMIIB domains important for filament assembly and the proteins used in this study. (A) The NMII molecule is a heterohexamer composed of two heavy chains, two essential light chains, and two regulatory light chains. The tail domain is an α-helical coiled-coil forming rod that is responsible for the assembly of NMII monomers into filaments (Vicente-Manzanares et al., 2009). Amino acids 1772–1856 and 1901–1933 are the NMIIB (MYH10) cACD and ACD domains, respectively. The cACD contains a negatively charged region (NCA/SBD, amino acids 1827–1833), and the ACD contains a positively charged region (amino acids 1925–1930) (Straussman, 2005). The 98-amino-acid distance between the positively charged region in ACD and the negatively charged region in cACD equals the stagger between every two NMII molecules that build a parallel filament (Huxley, 1957). Red and blue indicate negatively and positively charged amino acids, respectively. (B–D) Schematic illustration of NMIIB and survivin proteins used in this study. (E) The SBD sequence is conserved between NMII forms. Negatively charged amino acids are shown in red.

et al., 2010), and it undergoes phosphorylation and acetylation, which affect its functions (Aljaberi et al., 2015; Barrett et al., 2011, 2009; Colnaghi and Wheatley, 2010; O'Connor et al., 2000; Wheatley et al., 2007, 2004). It is not fully understood, however, how these modifications regulate the activity of survivin during mitosis. X-ray crystallography data have shown that survivin forms a stable homodimer in solution (Chantalat et al., 2000; Sun et al., 2005; Verdecia et al., 2000), but definitive evidence that this structure is needed for survivin function(s) *in vivo* is still lacking. By contrast, there is evidence that survivin interacts as a monomer with other CPC components (Bourhis et al., 2007; Jeyaprakash et al., 2007). Thus, it is not completely clear whether survivin functions as a monomer or as a homodimer *in vivo* (Engelsma et al., 2007; Pavlyukov et al., 2011).

In the present paper, we report for the first time that survivin forms a complex with NMII isoform B (NMIIB; i.e. the NMII heavy chain encoded by *MYH10*) *in vivo* through direct interactions, which impairs the ability of NMIIB to assemble into filaments. Combined live imaging and immunofluorescence analyses indicate that survivin and NMIIB colocalize mainly during telophase. We further provide evidence that the survivin–NMIIB interaction is essential for cytokinesis, and it is negatively regulated by Cdk1-mediated phosphorylation of survivin. Finally, only survivin in homodimers interacts with NMIIB. Our results indicate that survivin plays a crucial role in the regulation of NMIIB during cytokinesis, providing a mechanism for the precise and timely coordination of chromosomal and cytoskeletal events that are required for successful cell division.

RESULTS

Survivin and NMIIB form a complex *in vivo* through direct interaction, interfering with NMIIB filament assembly

Because survivin and NMIIB are essential for cytokinesis (Bao et al., 2005; Yang et al., 2004), we sought to analyze the relationship between them. We hypothesized that survivin and NMIIB might bind, providing a link between the CPC and the cytoskeleton. To test this hypothesis, HeLa cells expressing GFP–survivin were subjected to a co-immunoprecipitation assay with endogenous NMIIB. We found that GFP–survivin, but not GFP, co-immunoprecipitated with endogenous NMIIB, indicating the specificity of the interaction (Fig. 2A). Next, we sought to determine whether this interaction is direct. For this purpose, increasing concentrations of recombinant His-tagged survivin (His–survivin) were incubated with constant concentration of recombinant NMIIB rod fragment (Rod-B, Fig. 1B) and subjected to a direct pulldown assay. We found that Rod-B binds to survivin directly, with a dissociation constant (K_d) of 3.2±1.05 µM (mean±s.d.) (Fig. 2B).

Several studies have shown that NMII-binding proteins affect the ability of NMII to assemble into filaments (Dahan et al., 2012;

Journal of Cell Science (2019) 132, jcs233130. doi:10.1242/jcs.233130

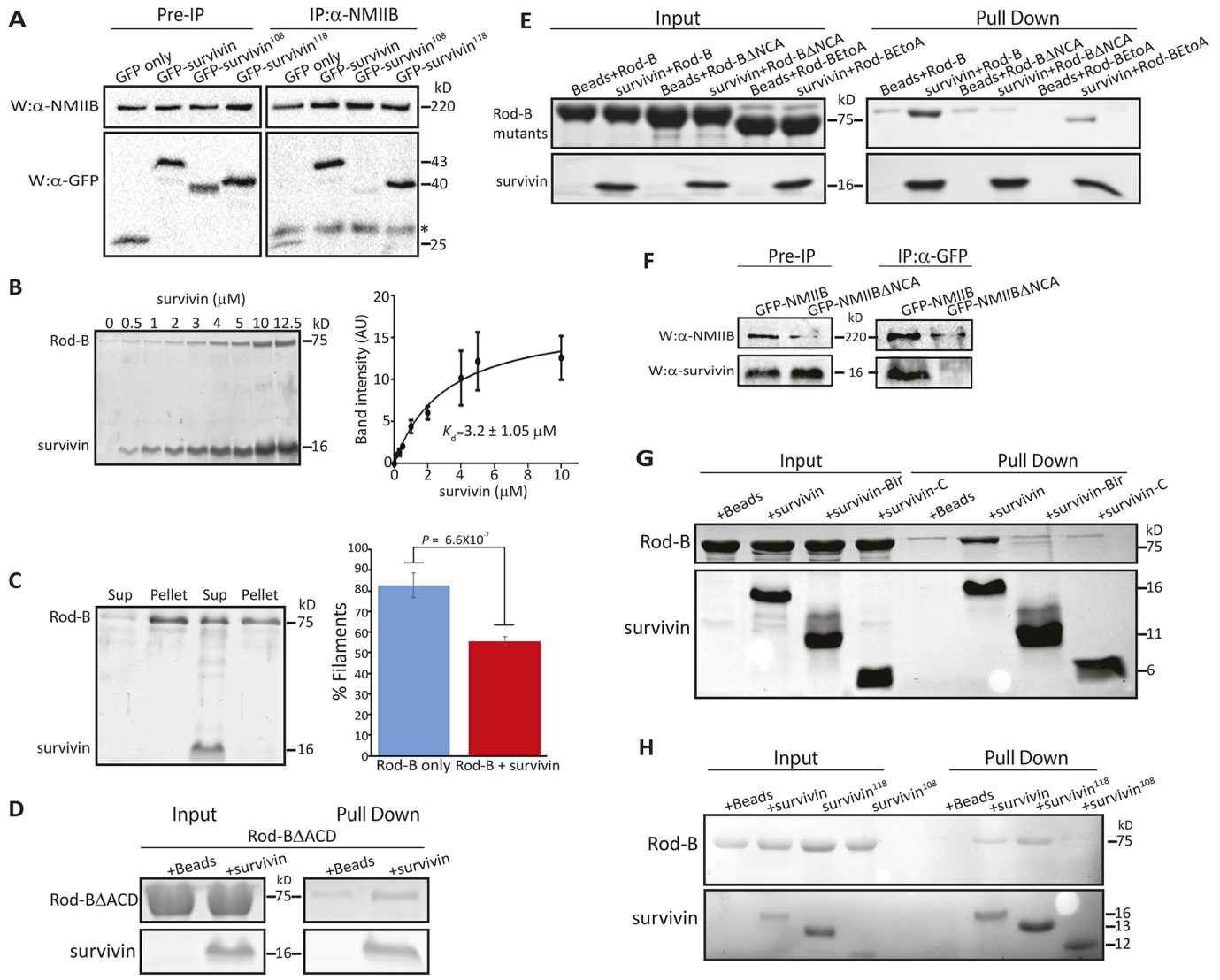

Fig. 2. Survivin and NMIIB form a complex *in vivo* through a direct interaction that interferes with NMIIB filament assembly. (A) GFP–survivin, GFP–survivin^{108} and GFP–survivin^{118} were expressed in HeLa cells and co-immunoprecipitated with endogenous NMIIB using anti-NMIIB antibody. The immunoprecipitated (IP) proteins were analyzed by immunoblotting (W) with antibodies against NMIIB and GFP. GFP only was used as a negative control. The asterisk indicates a non-specific band. (B) Left, increasing concentrations of recombinant His–survivin bound to Ni^{2+}-NTA beads were incubated with 0.5 µM Rod-B and analyzed on Coomassie-stained SDS-PAGE gels. Right, quantification of the binding signal of Rod-B to survivin. Rod-B bound to survivin with a K_d of 3.2 ±1.05 µM. Results are mean±s.d., *n*=3. (C) Rod-B alone and Rod-B in the presence of survivin were subjected to filament assembly assay and analyzed on Coomassie-stained SDS-PAGE gels. The extent of filament assembly was quantified by calculating the amount of Rod-B in the supernatant (sup) and pellet. Data represent mean±s.d. of six independent experiments. A two-tailed Student's *t*-test was used for statistical analysis. (D,E) Rod-B mutant proteins were mixed with survivin immobilized on Ni^{2+}-NTA beads, and the proteins were subjected to a pulldown assay. Coomassie-stained SDS-PAGE gels of His–survivin and Rod-B and Rod-BΔACD (D), and Rod-B, Rod-BΔNAC and Rod-B^{EtoA} (E). Ni^{2+}-NTA beads served as negative control. (F) Cos-7 cells depleted for NMIIB were transfected with HA–survivin and GFP–NMIIB or GFP–NMIIBΔNAC, and subjected to co-immunoprecipitation assay using GFP antibodies. The immunoprecipitated proteins were analyzed by immunoblotting with antibodies against NMIIB and survivin. (G) Coomassie-stained SDS-PAGE gels showing His–survivin, His–survivin fragments and Rod-B that were subjected to a pulldown assay as in D. (H) Coomassie-stained SDS-PAGE gels of Rod-B and His–survivin, His–survivin^{108} or His–survivin^{118} subjected to pulldown assay as in D.

Li et al., 2003). We therefore tested whether survivin binding to Rod-B affects its ability to form filaments. To this end, we induced Rod-B in monomers to assemble into filaments in the presence of survivin. At a molar ratio of two survivin units per Rod-B unit, only ∼55% of the Rod-B assembled into filaments, compared with ∼82% of Rod-B in filaments (Fig. 2C). Survivin was detected only in the supernatant (Rod-B monomers) and not in the pellet (filamentous Rod-B). Together, these results suggest that survivin binds to the Rod-B monomer and reduces its ability to form filaments.

The survivin-binding domain in NMIIB resides within a region important for filament assembly

The findings that survivin interferes with NMIIB filament assembly suggest that the survivin-binding domain in NMIIB lies within a region important for filament assembly. Previous studies identified regions along the NMII tail that are critical for filament formation. A highly conserved region near the C-terminal end of NMII, was termed the assembly competence domain or ACD (Fig. 1A; Cohen and Parry, 1998; Sohn et al., 1997; Straussman, 2005). Previous studies in our laboratory have identified a region N-terminal to

Journal of Cell Science (2019) 132, jcs233130. doi:10.1242/jcs.233130

ACD, also important for filament assembly, which we termed complementary ACD (cACD, Fig. 1A; Straussman, 2005). The ACD and cACD regions contain short stretches of positively and negatively (NCA) charged amino acids, respectively (Fig. 1A). We hypothesized that survivin binds to ACD or cACD, disrupting the filament assembly process of NMIIB. To test this hypothesis, we created recombinant Rod-B proteins missing the ACD or the NCA domains, denoted Rod-BΔACD and Rod-BΔNCA, respectively (Fig. 1B). We found that Rod-BΔACD but not Rod-BΔNCA interacted with survivin specifically (Fig. 2D,E). To characterize the nature of Rod-B–survivin interaction, we replaced the negatively charged amino acids in NCA with alanine residues (Rod-B^{EtoA}; Fig. 1B), and tested its ability to interact with survivin. We found a ∼70% reduction in the ability of Rod-B^{EtoA} to bind survivin (Fig. 2E), indicating that the interaction between survivin and Rod-B is at least partially electrostatic. To assess whether NCA are also important for the NMIIB interaction with survivin *in vivo*, we tagged full-length NMIIB that is missing the NCA domain with GFP (GFP–NMIIBΔNCA, Fig. 1C), and subjected it to co-immunoprecipitation assay with HA–survivin. To avoid the formation of heterofilaments between exogenous GFP–NMIIBΔNCA and endogenous NMIIB, which may bind HA–survivin, we used a Cos-7 cell line that does not express endogenous NMIIA (the NMII heavy chain encoded by *MYH9*) (Bao et al., 2005), and depleted NMIIB in this through inducible knockdown of NMIIB gene expression, because NMIIB is essential for cell proliferation (Bao et al., 2005). We found that GFP–NMIIB but not GFP–NMIIBΔNCA co-immunoprecipitated with HA–survivin (Fig. 2F). Together, these results indicate that the NMIIB residues E^{1827}EQLEQE^{1833} are required for survivin binding both *in vitro* and *in vivo*, and named this region the survivin-binding domain (SBD, Fig. 1A).

Determination of minimal survivin domain that binds NMIIB

To define the region of survivin that mediates its interaction with NMIIB, we generated recombinant His-tagged survivin-BIR and C-terminal α-helix domains (Fig. 1D). Neither of the survivin domains interacted with Rod-B in pulldown assay (Fig. 2G). We therefore extended the survivin-BIR domain to obtain two recombinant proteins containing the BIR domain and an additional 10 and 20 amino acids derived from the C-terminal α-helix domain, denoted survivin^{108} and survivin^{118}, respectively (Fig. 1D). We found that survivin^{118} but not survivin^{108} interacted with NMIIB specifically, both *in vivo* and *in vitro* (Fig. 2A,H). In addition, deletion of 30 amino acids from the survivin N-terminal domain (survivin$^{31–142}$) failed to bind Rod-B (data not shown). Together, these results indicate that survivin amino acids 1–118 are the minimal domain required for interaction with NMIIB.

Survivin and NMIIB colocalize during late phases of mitosis

To understand where and when the NMIIB–survivin interaction occurs during mitosis, we immunostained fixed HeLa cells for endogenous NMIIB and survivin, and quantified their fluorescence intensity at the equator. In metaphase and anaphase, survivin was localized mainly at the cell center, whereas NMIIB was mainly cytoplasmic, with some of it cortical. The two proteins did not exhibit colocalization (Fig. 3A–C; Fig. S1A). In early telophase, however, survivin was mainly located at the spindle midzone, and appeared also at the cell cortex, in the cleavage furrow, forming a ring-like structure as viewed in volume projection (*yz* dimensions) and 3D reconstruction (Fig. 3A–C; Fig. S1A). NMIIB was mainly concentrated at the cleavage plane forming the contractile ring, with some diffused in the midzone (Fig. 3A–C; Fig. S1A). Thus, in early telophase, survivin and NMIIB mainly colocalized in the equatorial cortex and, to a lesser extent, in the midzone. In late telophase, survivin assumed a disk shape, whereas NMIIB maintained a ring-like structure, with reduced colocalization seen between them (Fig. 3B). In cytokinesis, the survivin disk became smaller, and the NMIIB ring became constricted, with minimal colocalization between NMIIB and survivin (Fig. 3A–C; Fig. S1A). The seeming colocalization of NMIIB and survivin in cytokinesis (Fig. 3A) may result from the confinement of NMIIB and survivin to a narrow region in the cleavage furrow. Indeed, the 3D reconstruction shows a negligible degree of NMIIB and survivin colocalization (Fig. 3C).

To analyze the level of NMIIB and survivin colocalization, the Pearson's correlation coefficient (PCC) was calculated between the fluorescence intensity profiles of NMIIB and survivin in the equatorial cortex (Fig. S1B). Quantitatively, the PCC between NMIIB and survivin in early telophase (0.56±0.12; mean±s.d.) was significantly higher than in metaphase (0.11±0.09) and in late telophase (0.28±0.1) (Fig. 3D). Thus, survivin and NMIIB colocalize mainly in early telophase, and this colocalization is reduced as mitosis progress.

To determine the timing of survivin–NMIIB interaction, we tracked the localization of mCherry–survivin and GFP–NMIIB through cell division in live HeLa cells. In telophase, most of the GFP–NMIIB localized in the equatorial cortex, and some of it created a diffuse band in the cell midzone, whereas mCherry–survivin was localized mostly in the cell midzone, and some of it in the equatorial cortex (Fig. 3E; Movie 1). Thus, as revealed by the immunofluorescence images, in telophase mCherry–survivin and GFP–NMIIB colocalized mainly in the cell cortex and to some extent, in the cell midzone. As cytokinesis progressed, mCherry–survivin and NMIIB concentrated in the cell midbody. These results demonstrate the colocalization properties of survivin and NMIIB in live cells. Note that mCherry–survivin and GFP–NMIIB show a localization pattern similar to that of endogenous proteins, indicating that the expressed proteins mimic the characteristic localization profile of endogenous proteins.

To provide direct evidence that survivin and NMIIB interaction occurs after anaphase onset, we synchronized HeLa cells expressing mCherry–survivin to anaphase onset as determined by cyclin B degradation (Fig. 3F) and tubulin immunostaining (data not shown). These cells were subjected to co-immunoprecipitation assay with endogenous NMIIB. We found that the amount of survivin co-immunoprecipitated with NMIIB was ∼2-fold higher after anaphase onset as compared to before anaphase onset (Fig. 3F).

In sum, using immunofluorescence, live imaging and biochemical approaches, we showed that the highest degree of interaction between survivin and NMIIB occurs during telophase at the equatorial cortex, and to a lesser extent, at the cell midzone.

Depletion of survivin or NMIIB leads to cytokinesis defects

To further understand the importance of the interaction between NMIIB and survivin in mitosis, cells were depleted for NMIIB or survivin using the gene knockdown approach (Fig. S2A) and subjected to immunofluorescence staining. Depletion of NMIIB in HeLa cells, a cell line that expresses NMIIA and NMIIB (Maupin et al., 1994) did not present any significant phenotype, probably because NMIIA plays a role in cytokinesis (data not shown). In contrast, depletion of NMIIB in Cos-7 cells, a cell line that lacks NMIIA but contains NMIIB (Bao et al., 2005) caused multinucleation (Fig. 4A). These results indicate that NMIIB is

Journal of Cell Science (2019) 132, jcs233130. doi:10.1242/jcs.233130

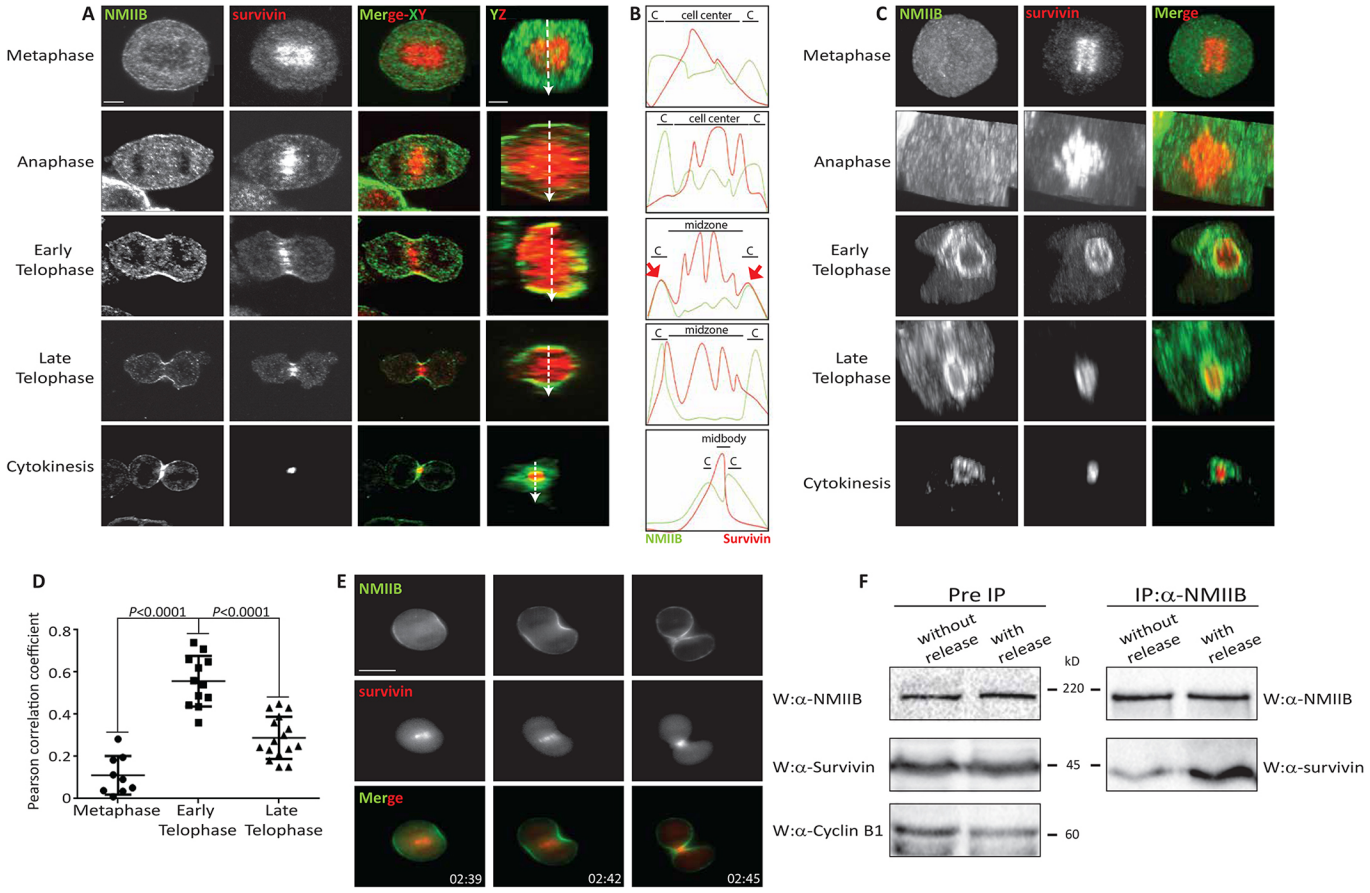

Fig. 3. Survivin and NMIIB colocalize during telophase. (A) HeLa cells were seeded on PDL coverslips, fixed, and immunostained for endogenous NMIIB (green) and survivin (red). Shown are single *z*-plane micrographs (*xy*) and volume projections of survivin and NMIIB in *yz* dimensions throughout mitosis. Tubulin was used to determine the mitotic stage of each cell (not shown). Scale bar: 2.5 µm. (B) Normalized fluorescent intensity was measured along the white dashed arrows shown in A. Colocalization is indicated by the red arrows, c, cell cortex. (C) 3D reconstitution of survivin (red) and NMIIB (green) localization in HeLa cells shown in A. (D) Pearson correlation coefficient between the fluorescence intensity of endogenous NMIIB and survivin in the cell cortex of metaphase cells and in the equatorial cortex of early and late telophase cells as shown in Fig. S1B. Results are mean±s.d., *n*=9, 12 and 16, respectively. (E) Single *z*-plane micrographs taken from a time-lapse movie of HeLa cells transiently expressing GFP–NMIIB and mCherry–survivin (Movie 1). Images were taken every 3 min. Scale bar: 10 µm. (F) Expression of mCherry–survivin was induced in HeLa-VPR mCherry–survivin cell line using doxycycline. Cells were synchronized with STLC followed by mitotic shake off. Half of the cells were lysed immediately ('no release') and the other half was released to a fresh medium without STLC for 3 h before lysis ('with release'). Cell extracts were subjected to co-immunoprecipitation using antibodies against NMIIB. The immunoprecipitated proteins were analyzed using antibodies against NMIIB and survivin. Cyclin B1 levels were used to determine the mitotic stage of the cells.

indispensable for cytokinesis in Cos-7 cells. HeLa cells, as well as Cos-7 cells, depleted for survivin became multinucleated (Fig. 4A; Fig. S2B). Similar results have been obtained using RPE cells and fibroblasts (Yang et al., 2004). Thus, survivin plays an essential role in cytokinesis in mammalian cells.

Although most HeLa cells depleted for survivin (survivin^{KD} cells) did not go through cytokinesis and became multinucleated, some cells expressed low amounts of survivin and were able to continue through later stages of mitosis. These cells exhibited cytokinesis defects, such as elongated intracellular bridge (Fig. 4B). In comparison to what was seen in control cells, NMIIB in these cells was diffused throughout the cells. Plotting the percentage of NMIIB and percentage survivin recruited to the equatorial cortex in control cells and in survivin^{KD} cells having residual survivin, revealed a linear correlation between the two proteins, suggesting that they depend on one another for recruitment to the equatorial cortex (Fig. 4C). Analysis of the percentage of NMIIB and survivin accumulation in the equatorial cortex of survivin^{KD} cells showed reduced recruitment of both proteins (Fig. 4D), although the expression of NMIIB was not affected by the depletion of survivin (Fig. S2A). Together, these results indicate that survivin and NMIIB are essential for cytokinesis and depend on each other for recruitment to the equatorial cortex.

The interaction between survivin and NMIIB is required for mitosis

To study the importance of the direct interaction between survivin and NMIIB for cytokinesis, we expressed GFP–NMIIB that is missing the survivin-binding domain (GFP–NMIIBΔSBD, Fig. 1C) and mCherry–survivin in HeLa cells, and tracked the cellular properties of these proteins throughout mitosis. Remarkably, these cells exhibited defects in mitosis; ∼45% of the cells attempted to undergo bipolar cytokinesis, but the daughter cells in cytokinesis did not separate and underwent furrow regression (Fig. 5A; Movie 2). GFP–NMIIBΔSBD appeared to over-accumulate at the cell cleavage furrow. Indeed, while ∼13% of GFP–NMIIB or

Journal of Cell Science (2019) 132, jcs233130. doi:10.1242/jcs.233130

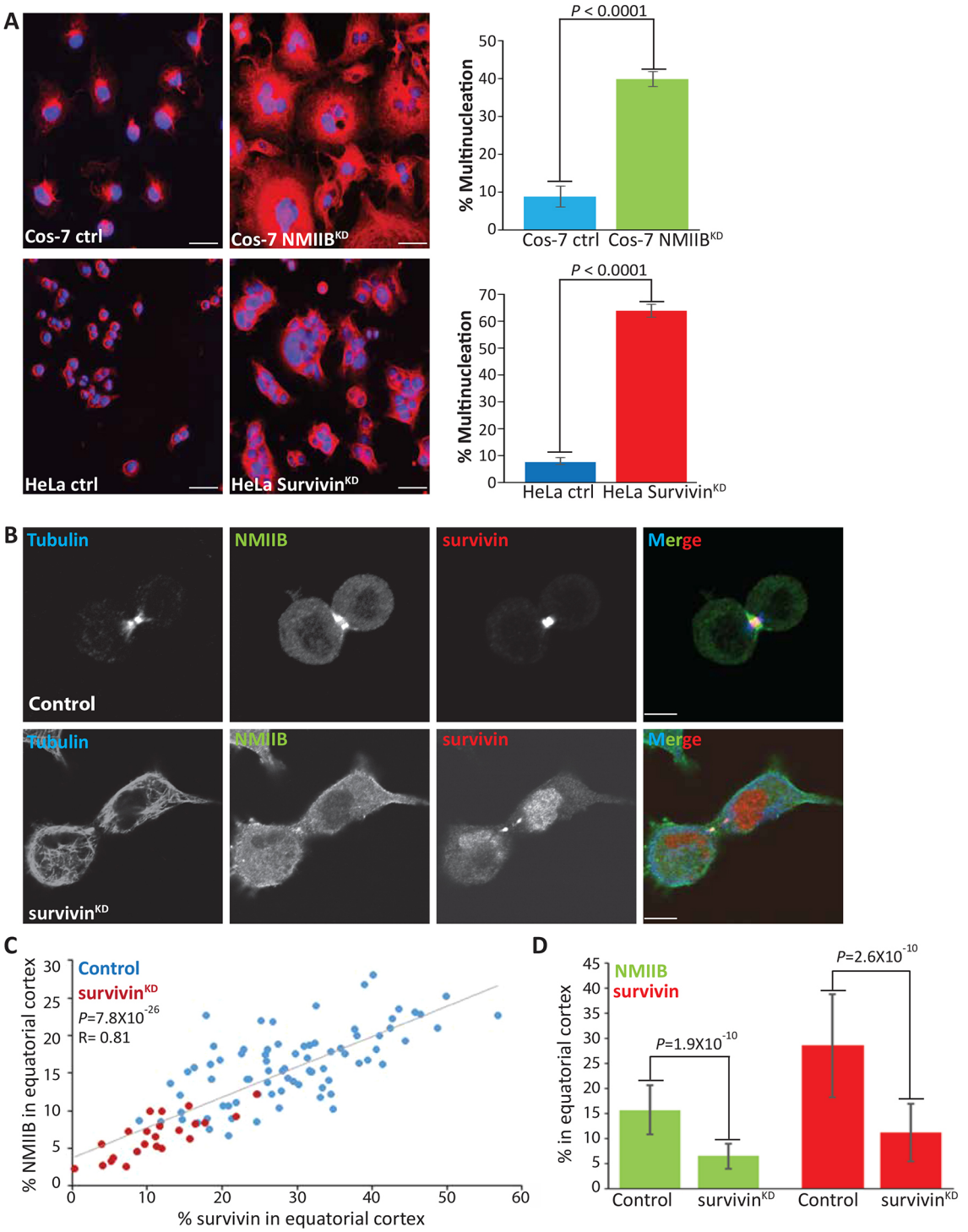

Fig. 4. The effect of survivin and NMIIB depletion on mitosis. (A) Cos-7 cells depleted for NMIIB (Cos-7 NMIIB^{KD}, upper panel) and HeLa cells depleted for survivin (HeLa survivin^{KD}, lower panel) were stained for microtubules (red) and DAPI (blue). Right, quantification of multinucleation in Cos-7-NMIIB^{KD} (upper panel) and HeLa survivin^{KD} (lower panel). Results are mean±s.d., n≥800. Scale bars: 50 µm. (B) HeLa control cells and HeLa survivin^{KD} cells were immunostained for tubulin (blue), NMIIB (green) and survivin (red). Survivin staining of survivin^{KD} cells was used to differentiate between cells that partially express survivin and those in which survivin has been completely knocked down. Tubulin was used to determine the mitotic stage of the cell. (C) Survivin and NMIIB enrichments in the equatorial cortex are correlated with one another. The percentage of survivin and NMIIB in the equatorial cortex was calculated by dividing the intensity of the fluorescence of these proteins in the equatorial cortex by the intensity of the fluorescence of each protein in the entire cell. n=105. The P-value for the Pearson correlation coefficient was calculated. (D) The percentage of NMIIB (green) and survivin (red) recruited to the equatorial cortex in control and survivin^{KD} cell lines was determined as in C. Data represent the mean±s.d. of n=105. A two-tailed Student's t-test was used for statistical analysis. Scale bars: 10 µm.

Journal of Cell Science (2019) 132, jcs233130. doi:10.1242/jcs.233130

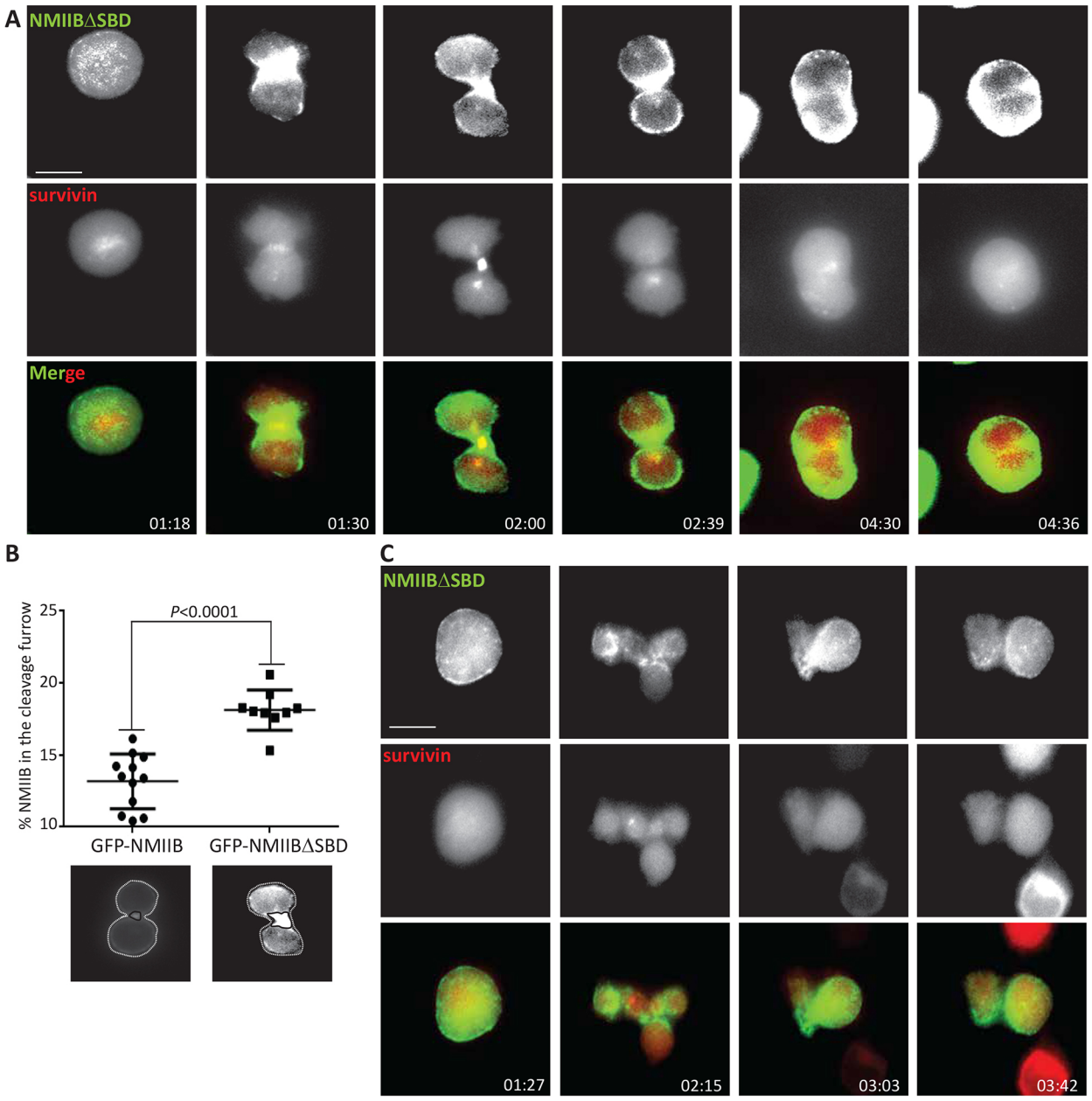

Fig. 5. NMIIB missing the survivin-binding domain is highly enriched in the cleavage furrow, causing mitotic defects. (A,C) Single *z*-plane micrographs taken from time-lapse movies of HeLa cells transiently expressing GFP–NMIIBΔSBD and mCherry–survivin (Movies 2 and 3). Images were taken every 3 min. In some cells, the cleavage furrow regressed (A), whereas other cells had many cleavage furrow sites (C). Scale bars: 10 µm. (B) The percentage of GFP–NMIIB proteins in the cleavage furrow was determined by dividing the fluorescence intensity of GFP–NMIIB proteins in the cleavage furrow (confined by the black line) by the fluorescence intensity of these proteins in the entire cell (confined by the doted white line). Data represent mean±s.d. of n=12 for cells expressing GFP–NMIIB and n=9 cells expressing GFP–NMIIΔSBD. A two-tailed Student's *t*-test was used for statistical analysis.

endogenous NMIIB accumulated at the cleavage furrow, ∼18% of GFP–NMIIBΔSBD accumulated in this region (Fig. 5B). mCherry–survivin appeared to localize at the cell midbody, but as the cell underwent fusion, it mislocalized and seemed to concentrate in the cell center. To test whether the over-accumulation of GFP–NMIIBΔSBD at the cell cleavage furrow is the result of its overexpression or filament over-assembly because of the absence of the SBD, we determined the expression levels of GFP–NMIIBΔSBD and compared it to GFP–NMIIB as well as the filament assembly capabilities of Rod-BΔSBD (Fig. 1B). We found that the expression levels of GFP–NMIIBΔSBD and GFP–NMIIB were similar (Fig. S3A). In physiological salt conditions, Rod-BΔSBD formed filaments to a similar extent to Rod-B, indicating that deletion of SBD did not affect the intrinsic filament assembly properties of GFP–NMIIBΔSBD (Fig. S3B). Thus, the over-accumulation of GFP–NMIIBΔSBD was the result of the absence of the survivin–NMIIB interaction. Note that deletion of the cACD that contains the SBD (Rod-BΔcACD, Fig. 1B) yielded filament-assembly-incompetent Rod-B (Fig. S3B), indicating that the SBD resides within a region important for NMIIB filament assembly. Thus, survivin binding to SBD may mask this region, hindering NMIIB filament assembly.

Together, these results may indicate that in the absence of NMIIB–survivin interaction, NMIIB filament assembly at the cleavage furrow is unregulated, leading to filament over-assembly and mitosis defects.

Approximately 20% of the cells expressing GFP–NMIIBΔSBD exhibited multipolar mitosis with multiple ingression sites, generating several asymmetric daughter cells linked by an intracellular bridge, with GFP–NMIIBΔSBD forming a contractile ring-like structure at the base of these cells (Fig. 5C; Movie 3). These cells remained either separated or fused during cytokinesis. mCherry–survivin was diffused throughout the multipolar mitosis, indicating that intact NMIIB is required for the correct cellular localization of survivin during mitosis. In some cells, furrows were seen while survivin was still organized in puncta, which is indicative of early mitotic stages, such as metaphase (data not shown).

Together, these results suggest that the survivin–NMIIB interaction is important for the regulation of the spatio-temporal formation of the contractile ring. When the interaction is disturbed, survivin is unable to regulate NMIIB filament assembly, resulting in incorrect localization and timing of NMIIB filament formation.

The survivin–NMIIB interaction is regulated by phosphorylation of survivin by Cdk1

During mitosis, survivin is phosphorylated by the mitotic kinase Cdk1 at threonine 34 (phospho-survivin^{T34}) (O'Connor et al., 2000). Expression of phosphoresistant or phosphomimetic survivin mutants, survivin^{T34A} and survivin^{T34D}, respectively, affect cell growth (Barrett et al., 2009), indicating that Cdk1-mediated phosphorylation of survivin affects the cell cycle. Therefore, we tested whether phosphorylation of survivin by Cdk1 affects its interaction with NMIIB. First, we tested the effect of the Cdk1-specific inhibitor RO-3306 on survivin–NMIIB complex formation *in vivo*. To this end, HeLa cells were treated with RO-3306, and endogenous survivin and NMIIB were subjected to the co-immunoprecipitation assay. Only survivin from RO-3306-treated cells co-immunoprecipitated with NMIIB (Fig. 6A), indicating that Cdk1 phosphorylation of survivin interferes with the survivin–NMIIB interaction. Next, using antibodies specific for phospho-survivin^{T34}, we tested whether survivin that co-immunoprecipitated with NMIIB is phosphorylated by Cdk1. Because these antibodies recognize only recombinant phospho-survivin^{T34}, HeLa cells expressing GFP–survivin were subjected to co-immunoprecipitation assay with endogenous NMIIB. We found that phospho-survivin^{T34} antibodies recognized the GFP–survivin in the cell extract but not in the GFP–survivin–NMIIB complex (Fig. 6B). These results confirmed that phospho-survivin^{T34} does not interact with NMIIB and that phosphorylation of survivin by Cdk1 regulates its interaction with NMIIB. To further study the role of Cdk1 phosphorylation of survivin on its interaction with NMIIB, we tested whether survivin^{T34A} and survivin^{T34D} interact with NMIIB. We found that GFP–survivin and GFP–survivin^{T34A} formed a complex with endogenous NMIIB; however, GFP–survivin^{T34D} did not (Fig. 6C). A pulldown assay indicated that survivin^{T34A} and survivin^{T34D} interacted to a lesser extent with Rod-B compared to survivin (Fig. 6D). Thus, survivin phospho-mutants exhibited impaired binding to NMIIB. Note that survivin is phosphorylated by several other kinases: polo-like kinase 1 at serine 20 (Colnaghi and Wheatley, 2010), casein kinase at threonine 48 (Barrett et al., 2011), and Aurora B at threonine 117 (Wheatley et al., 2007), but these sites do not seem to be involved in the regulation of the survivin–NMIIB interactions (data not shown). Cdk1 inactivation is required for anaphase onset (Chang et al., 2003). To explore the role of survivin phosphorylation by Cdk1 on its interaction with NMIIB during mitosis, we determined the amount of phospho-survivin^{T34} before and after anaphase onset. We found that the level of phospho-survivin^{T34} was ∼3-fold higher before anaphase onset (Fig. 6E). These results are consistent with the findings that unphosphorylated survivin interacts with NMIIB (Fig. 6A,B), and that survivin and NMIIB colocalize during telophase (Fig. 3). Next, we analyzed the cellular localization of phospho-survivin^{T34} and NMIIB during mitosis, and found that there is minimal colocalization between phospho-survivin^{T34} and NMIIB throughout mitosis (Fig. 6F). Together, these results may indicate that phosphorylation of survivin by Cdk1 before anaphase onset ensures that the contractile ring is initiated only after anaphase onset.

To explore the functional significance of survivin phosphorylation by Cdk1 on mitosis, we expressed mCherry–survivin^{T34D} and GFP–NMIIB in HeLa cells and subjected them to live-cell imaging. mCherry–survivin^{T34D}-expressing cells exhibited bipolar, tripolar and multipolar mitoses – similar phenotypes to those of cells expressing GFP–NMIIBΔSBD. In bipolar mitotic cells (∼30% of mCherry–survivin^{T34D} cells), mCherry–survivin^{T34D} and GFP–NMIIB seemed to colocalize at the midbody. However, since phosphomimetic survivin did not bind to NMIIB both *in vivo* and *in vitro*, it is plausible that mCherry–survivin^{T34D} and NMIIB reside in overlapping regions but they do not interact. The daughter cells of the bipolar mitotic cells did not separate and underwent furrow regression (Fig. 6G; Movie 4). ∼30% of mCherry–survivin^{T34D} cells exhibited tripolar mitosis, and the daughter cells underwent furrow regression (Fig. 6H; Movie 5). In addition, in these cells, GFP–NMIIB over-assembled at the base of the daughter. Quantification of the proportion of GFP–NMIIB at various locations showed that ∼13% of GFP–NMIIB accumulated in the cleavage furrow of control cells, whereas ∼18% of GFP–NMIIB accumulated at this location in mCherry–survivin^{T34D} cells (Fig. 6I); ∼30% of cells expressing mCherry–survivin^{T34D} exhibited multipolar mitosis with diffused GFP–NMIIB and mCherry–survivin^{T34D}, and the daughter cells underwent furrow regression (Fig. S4A; Movie 6). These phenotypes were not the results of mCherry–survivin^{T34D} overexpression (Fig. S4B). These results may indicate that, in the absence of the survivin–NMIIB interaction, NMIIB filament assembly is unregulated, leading to mitosis defects, highlighting the importance of survivin phosphorylation by Cdk1 for the regulation of NMIIB during mitosis.

Survivin dimerization is necessary for NMIIB interaction and proper mitosis

Survivin^{118} but not survivin^{108} directly interacted with NMIIB (Fig. 2A,H). Because survivin^{118} and not survivin^{108} formed homodimers (Fig. S5A), we speculated that survivin dimerization is important for NMIIB binding. Structural studies indicate that survivin has two dimerization interfaces, utilizing residues leucine 6 (L6) and tryptophan 10 (W10), and phenylalanine 101 (F101) and leucine 102 (L102) (Verdecia et al., 2000). Indeed, replacing F101 and L102 with alanine residues (survivin$^{F101A/L102A}$) led to a dimerization-incapable survivin mutant (Engelsma et al., 2007). However, there is no experimental data indicating that the L6 and W10 interface is needed for survivin homodimerization. We therefore analyzed the molecular mass of survivin in which residues L6 and W10 were replaced with alanine residues (survivin$^{L6A/W10A}$). We found that whereas survivin formed homodimers, survivin$^{L6A/W10A}$ and survivin$^{F101A/L102A}$ were monomers (Fig. 7A). Next, we tested whether these dimerization mutant survivin forms interacted with NMIIB. We found that neither protein interacted with NMIIB *in vivo* or *in vitro* (Fig. 7B,C).

Journal of Cell Science (2019) 132, jcs233130. doi:10.1242/jcs.233130

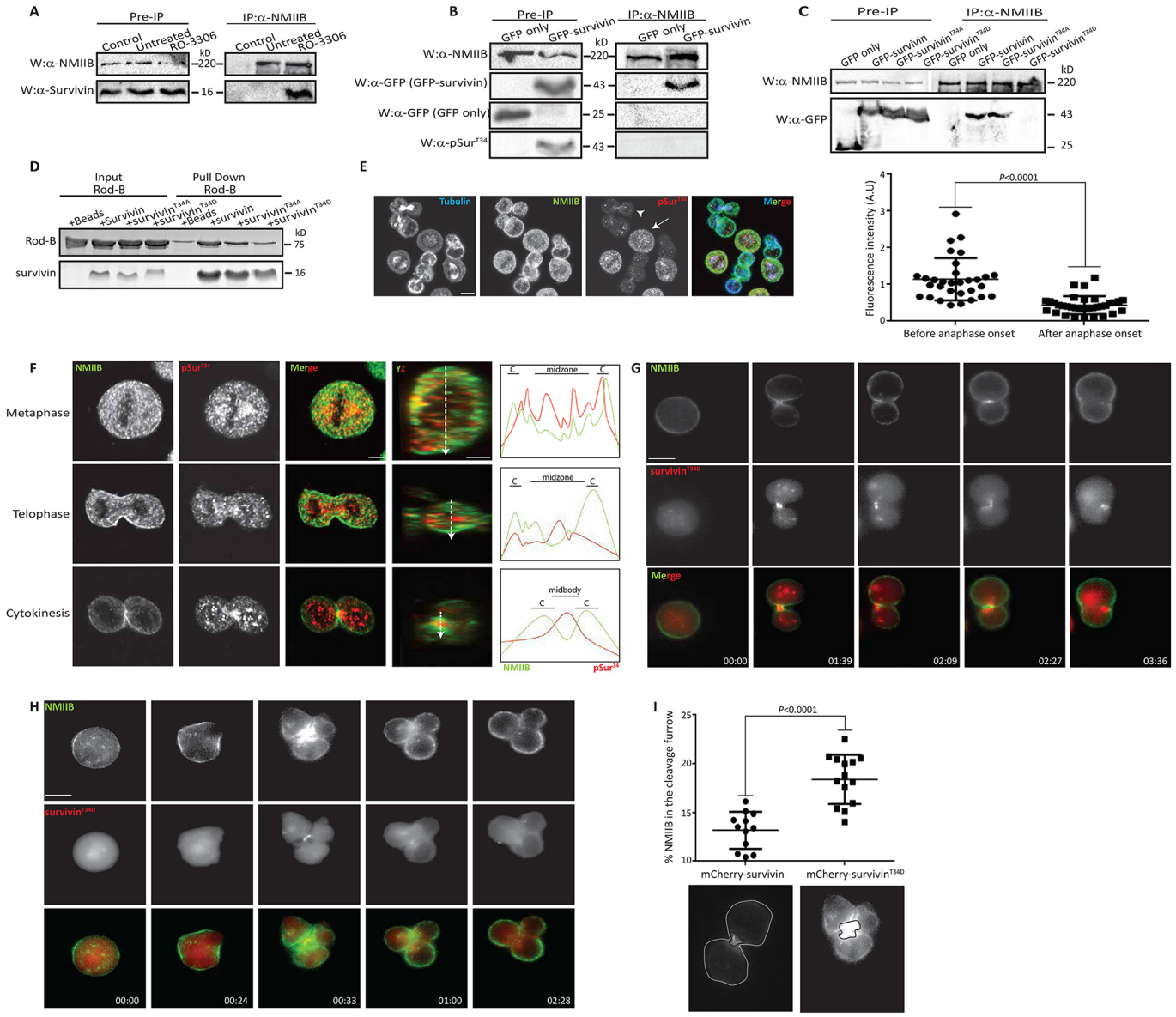

Fig. 6. The survivin–NMIIB interaction is negatively regulated by Cdk1-mediated phosphorylation. (A) HeLa cells were treated with the Cdk1 inhibitor RO-3306 for 1 h, and subjected to co-imunoprecipitation of endogenous survivin and NMIIB using anti-NMIIB antibody. The immunoprecipitated (IP) proteins were analyzed by immunoblotting (W) with antibodies against NMIIB and survivin. Protein A/G beads were used as negative control. (B) HeLa cells expressing GFP or GFP–survivin were subjected to a co-immunoprecipitation assay with endogenous NMIIB using anti-NMIIB antibody. The immunoprecipitated NMIIB was analyzed by immunoblotting with antibodies against NMIIB. The immunoprecipitated GFP and GFP–survivin were first immunoblotted with antibody against phospho-survivin^{T34} (pSur^{T34}). Then, the membrane was stripped and re-blotted with antibody against GFP. GFP only was used as a negative control. (C) 293T cells expressing GFP–survivin, GFP–survivin^{T34A} or GFP–survivin^{T34D} were subjected to a co-immunoprecipitation assay with endogenous NMIIB using anti-NMIIB antibody. The immunoprecipitated proteins were analyzed by immunoblotting with antibodies against NMIIB and GFP. GFP only was used as a negative control. (D) Coomassie-stained SDS-PAGE of Rod-B and His–survivin, His–survivin^{T34A} or His–survivin^{T34D} were subjected to a pulldown assay. Ni^{2+}-NTA beads served as a negative control. Because survivin dimerization is necessary for its interaction with NMIIB, we confirmed that survivin^{T34D} can form dimers (Fig. S5A). (E) Left, HeLa cells were seeded on PDL-coated coverslips, fixed, and immunostained for tubulin (blue), NMIIB (green) and pSur^{T34} (red). The arrow and arrowhead indicate metaphase and cytokinetic cells, respectively. Right, quantification of the relative amount of phospho-survivin^{T34} before and after anaphase onset. Results are mean±s.d., n=31 and 34, respectively. Scale bar: 10 µm. (F) HeLa cells were seeded on PDL, fixed and immunostained for NMIIB (green) and pSur^{T34} (red). Shown are single z-plane micrographs and volume projections of NMIIB and pSur^{T34} in yz dimensions throughout mitosis. Arrows represent the line scan of pSur^{T34} and NMIIB in the volume projection. Tubulin was used to determine the mitotic stage of each cell (not shown). Scale bars: 2.5 µm. C, cell cortex. (G,H) Single z-plane micrographs taken from time-lapse movies of HeLa cells transiently expressing GFP–NMIIB and mCherry–survivin^{T34D} (Movies 4 and 5). Some cells showed cleavage furrow ingression and cell fusion (G), whereas others showed tripolar mitosis and cell fusion (H). Scale bar: 10 µm. (I) The percentage of NMIIB recruited to the cleavage furrow was determined as in Fig. 5B. Data represent mean±s.d. of n=12 for cells expressing mCherry–survivin and n=14 for cells expressing mCherry–survivin^{T34D}. A two-tailed Student's t-test was used for statistical analysis.

These results indicate that survivin dimerization is necessary for NMIIB binding, and that only the survivin homodimer interacts with NMIIB.

To examine the effect of survivin dimerization on NMIIB and mitosis, we subjected HeLa cells expressing mCherry–survivin$^{F101A/L102A}$ or mCherry–survivin$^{L6A/W10A}$ and GFP–

Journal of Cell Science (2019) 132, jcs233130. doi:10.1242/jcs.233130

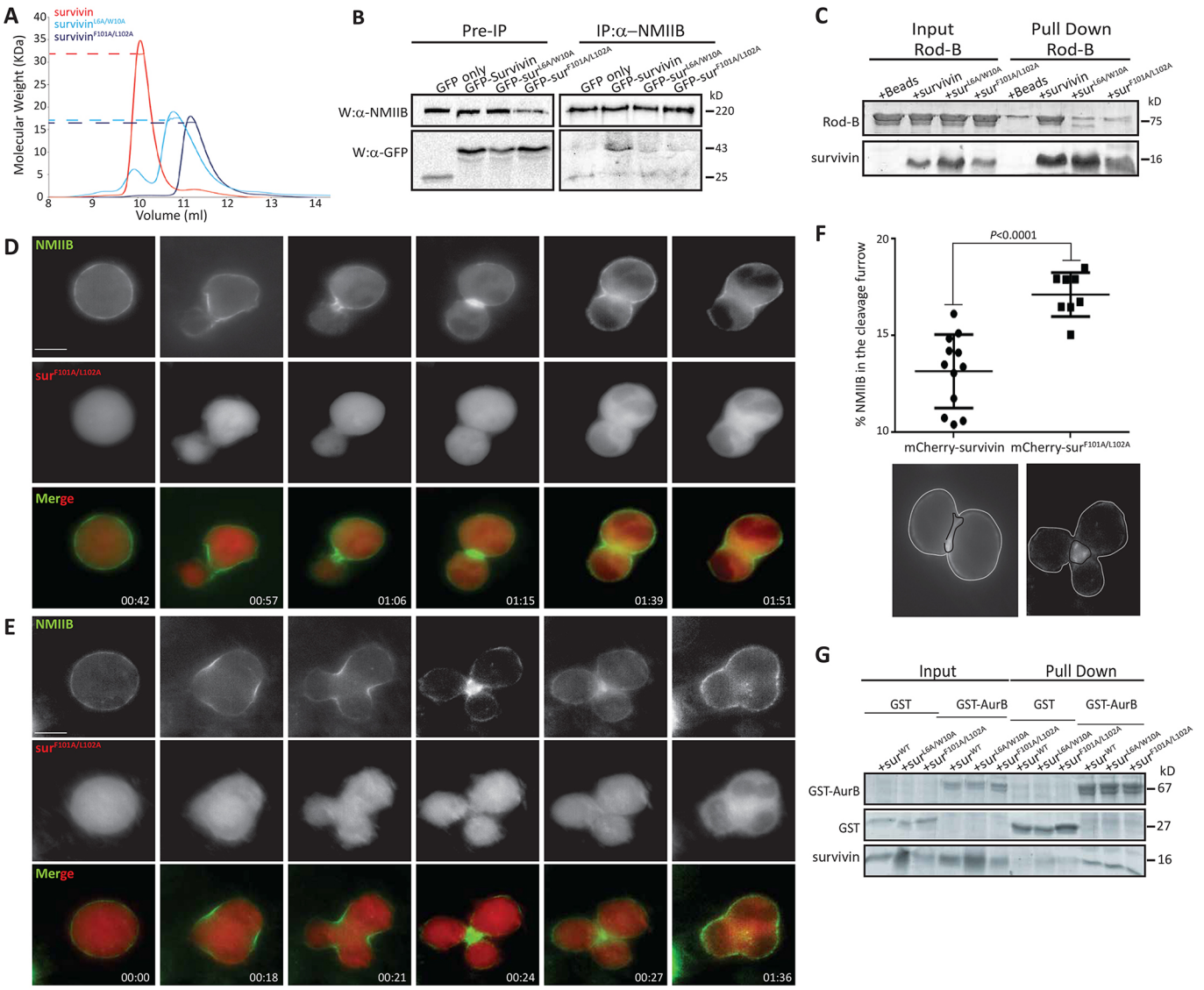

Fig. 7. Survivin dimerization is important for interaction with NMIIB. (A) The molecular mass of purified survivin proteins was determined by SEC-MALS. The molecular mass of survivin was ∼32 kDa and of survivin$^{L6A/W10A}$ and survivin$^{F101A/L102A}$ were ∼16 kDa. The calculated mass of survivin dimer and monomer are 35 and 18 kDa, respectively; therefore, survivin$^{L6A/W10A}$ and survivin$^{F101A/L102A}$ form monomers. (B) HeLa cells expressing GFP–survivin, GFP–survivin$^{F101/L102A}$ or GFP–survivin$^{L6A/W10A}$ were subjected to a co-immunoprecipitation assay with endogenous NMIIB using anti-NMIIB antibody, and analyzed as in Fig. 2A. (C) Coomassie-stained SDS-PAGE of Rod-B and His-survivin, survivin$^{F101/L102A}$ or survivin$^{L6A/W10A}$ subjected to a pulldown assay. Ni^{2+}-NTA beads served as a negative control. (D,E) Single *z*-plane micrographs taken from time-lapse movies of HeLa cells transiently expressing GFP–NMIIB and mCherry–survivin$^{F101/L102A}$ (Movies 7, 8). Cells showed cleavage furrow ingression followed by regression (C). Other cells went through tripolar mitosis (D). Scale bars: 10 µm. (F) The percentage of NMIIB recruited to the cleavage furrow was determined as in Fig. 5B. Data represent mean±s.d. of n=12 for cells expressing mCherry-survivin and n=8 for cells expressing mCherry-survivin$^{F101A/L102A}$. A two-tailed Student's *t*-test was used for statistical analysis. (G) GST or GST–Aurora-B (GST-AurB) immobilized on glutathione beads were mixed with His–survivin mutant proteins. The proteins were subjected to a pulldown assay and analyzed on Coomassie-stained SDS-PAGE gels.

NMIIB to live-cell imaging. Similar to what was seen in the GFP–NMIIBΔSBD and mCherry–survivin^{T34D} cell lines, the mCherry–survivin$^{F101A/L102A}$ and mCherry–survivin$^{L6A/W10A}$ cells formed bipolar and tripolar anaphases, and the daughter cells fused during cytokinesis (Fig. 7D,E; Fig. S5B and Movies 7–9). mCherry–survivin$^{F101A/L102A}$ and mCherry–survivin$^{L6A/W10A}$ were diffused throughout mitosis, whereas GFP–NMIIB in bipolar cells formed a contractile-ring-like structure that concentrated at the cleavage furrow, but the contractile ring disassembled without separating the daughter cells (Fig. 7D; Fig. S5B). In tripolar cells, similar to bipolar cells, mCherry–survivin$^{F101A/L102A}$ was diffused throughout mitosis, but in telophase-like stage NMIIB concentrated in three regions, whereas in cytokinesis-like stages it was concentrated in a center point where the three daughter cells were still connected. Quantification of GFP–NMIIB showed that ∼13% of GFP–NMIIB accumulated at the cleavage furrow of control cells, whereas ∼17% of GFP–NMIIB accumulated in mCherry–survivin$^{F101A/L102A}$ cells (Fig. 7F). These phenotypes were not the results of mCherry–survivin$^{L6A/W10A}$ or mCherry–survivin$^{F101A/L102A}$ overexpression (Fig. S4B). These observations indicate that the survivin dimerization status is important for its interaction with NMIIB and for proper mitosis.

Journal of Cell Science (2019) 132, jcs233130. doi:10.1242/jcs.233130

Survivin is essential for targeting the CPC to the centromere during mitosis (Kelly et al., 2010; Wang et al., 2010; Yamagishi et al., 2010). When INCENP, survivin or borealin localization and/or function are perturbed, the other subunits of the CPC do not localize properly, Aurora B activity is diminished and proper cell division is compromised (Carvalho et al., 2003; Honda et al., 2003; Vader et al., 2006). To test whether the phenotype presented by cells expressing survivin$^{L6A/W10A}$ or survivin$^{F101A/L102A}$ was due to their inability to bind to CPC, we examined whether these survivin mutant proteins formed a complex with the CPC protein Aurora B. We found that survivin$^{L6A/W10A}$ and survivin$^{F101A/L102A}$ formed a complex with Aurora B through direct interactions (Fig. 7G). Similar results were obtained with borealin (data not shown). These results indicate that monomeric survivin is capable of binding to the CPC and provide the first indication that survivin binds to CPC as a monomer. These results are in agreement with structural studies indicating that survivin recognizes the CPC through its dimerization domain, suggesting that it functions as a monomer in the complex (Jeyaprakash et al., 2007).

DISCUSSION

It has been well known for many years that the actomyosin ring is important for cytokinesis in many eukaryotic cells, but many questions remained open; for example, concerning the signals that initiate furrow ingression and the mechanism that allows NMII to assemble into filaments in the equatorial cortex only. Accumulating data indicate that the CPC regulates several processes in mitosis, including cytokinesis and abscission (Carmena et al., 2012); therefore, the CPC may play a yet unknown role early in contractile ring formation or function. Our results may answer some of these questions. We demonstrate that survivin interacts directly with NMIIB through a domain located within a domain essential for NMIIB filament assembly. We propose that survivin binding to NMIIB sequesters NMIIB monomers interfering with the assembly process (Fig. 8A). Note that the SBD is conserved among all NMII isoforms (Fig. 1E); therefore, survivin may bind to all NMII isoforms. Indeed, we found that survivin co-immunoprecipitated with NMIIA (data not shown), and therefore may also regulate NMIIA and NMIIC filament assembly.

Contractile ring formation must be regulated with spatial and temporal precision to ensure that the cleavage furrow is positioned properly. The temporal control of the contractile ring assembly is regulated by mitotic kinases to ensure that the contractile ring is initiated only after anaphase onset, after the chromosomes have separated (Wieser and Pines, 2015). Cyclin B–Cdk1 is the key regulator of cell cycle (Nurse, 1990), and for the cell to enter anaphase, cyclin B is degraded, inactivating Cdk1 (Chang et al., 2003). Cdk1 phosphorylates survivin (O'Connor et al., 2000), and we show that this phosphorylation takes place before anaphase

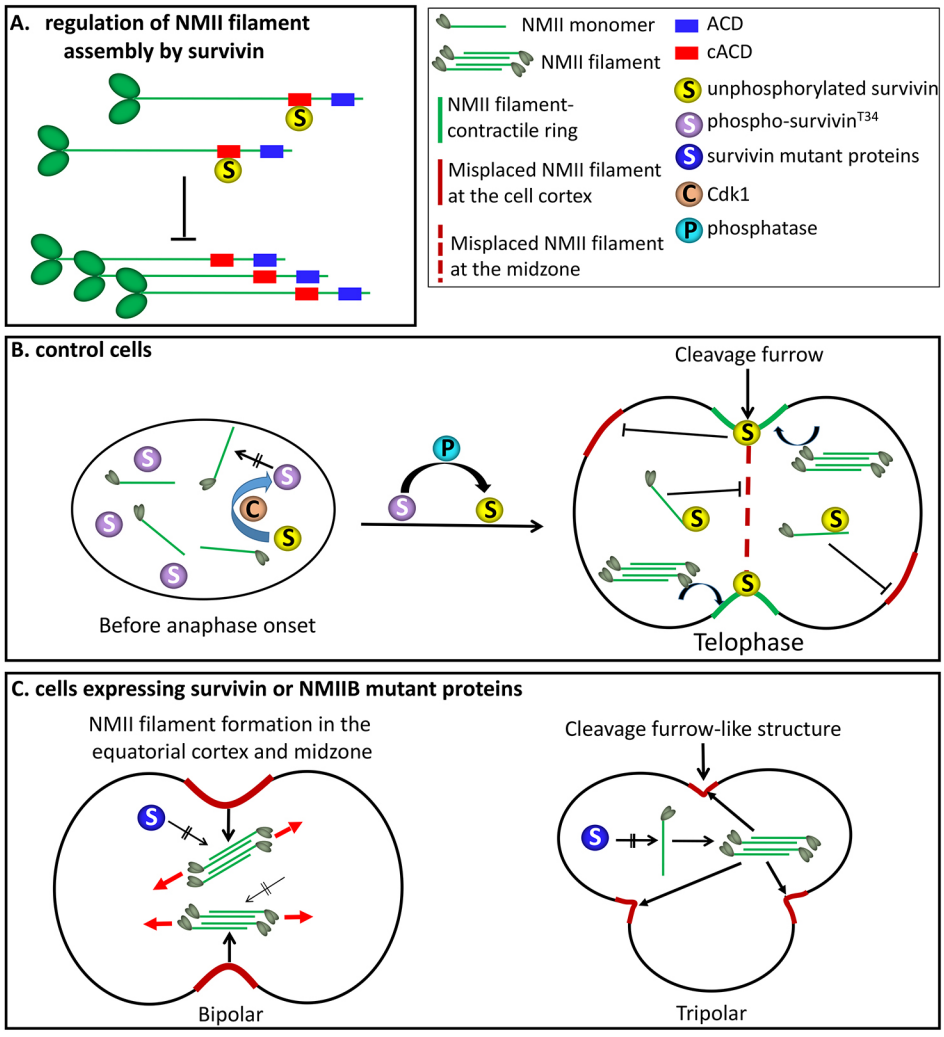

Fig. 8. The interaction between survivin and NMIIB is required for cytokinesis. (A) Survivin interferes with NMIIB filament assembly by binding to monomeric NMIIB in the cACD domain, preventing the interaction between NMIIB monomers to build the filament. (B) Before anaphase onset, Cdk1 is highly active and it phosphorylates survivin, preventing its interaction with NMIIB. At telophase, an unknown phosphatase removes the phosphate from the phospho-survivin^{T34}, allowing survivin to bind to NMIIB monomers in the cell cortex and midzone, preventing filament assembly at this region as well as in regions outside the equatorial cortex. NMIIB is recruited from the cytoplasm to the equatorial cortex to form the contractile ring. At the equatorial cortex, survivin is bound to some NMIIB molecules, regulating the number of NMIIB molecules that join the contractile ring, thus regulating the size of the ring. (C) Disruption of survivin–NMIIB interaction leads to unregulated NMIIB filament assembly and mitosis defects. Left, bipolar mitosis; in the absence of the survivin–NMIIB interaction, there is too high a level of NMIIB filament formation in the cell cortex and midzone, creating random contractile forces leading to ring regression and cell fusion. Black and red arrows indicate random contractile forces derived from NMIIB filaments in the cell cortex and midzone, respectively. Right, tripolar mitosis; in the absence of the survivin–NMIIB interaction, NMIIB forms aberrant filaments in different regions of the cell cortex, leading to cleavage furrow-like structures in multiple places and to multipolar cytokinesis and cell fusion.

Journal of Cell Science (2019) 132, jcs233130. doi:10.1242/jcs.233130

onset. The phosphorylated survivin does not interact with NMIIB. Indeed, we could detect an endogenous survivin–NMIIB complex only after inhibition of Cdk1. We showed further that survivin and NMIIB colocalize and interact mainly during telophase. Thus, Cdk1 inactivation before anaphase onset allows the formation of a survivin–NMIIB complex. We propose that, before anaphase onset, survivin is phosphorylated by Cdk1, preventing its binding to NMIIB (Fig. 8B). At telophase, when Cdk1 activity rapidly declines, an unknown phosphatase removes the phosphate from phospho-survivin^{T34}, allowing it to bind to NMIIB (Fig. 8B). During telophase, survivin colocalizes with NMIIB in the equatorial cortex, and to some extent at the midzone. Our data suggest that the interaction of survivin with NMIIB during telophase prevents the formation of the contractile ring in the midzone disk and in regions other than the equatorial cortex, by sequestering NMIIB monomers (Fig. 8B). In the equatorial cortex, survivin may regulate the number of NMIIB molecules that assemble into the contractile ring. It has been shown that NMII is recruited directly from the cytoplasm to the equatorial cortex (Zhou and Wang, 2008), and has been proposed that equatorial NMII filaments are either assembled from cytoplasmic monomers or through recruitment of preassembled filaments (Zhou and Wang, 2008). Thus, survivin may also regulate the contractile ring formation by releasing NMIIB monomers from the midzone survivin–NMIIB complex, and by recruiting these monomers to the growing NMII filaments (Fig. 8B). Previous studies have shown that the contractile ring is assembled when the active zone of RhoA at the equatorial cortex is formed (Bement et al., 2005). Rho-GTP activates ROCK, which elevates the phosphorylation of myosin light chains to promote NMII assembly and trigger its motor activity (Dean and Spudich, 2006). It was shown, however, that despite the inhibition of ROCK, NMII is present in the equatorial cortex (Zhou and Wang, 2008), suggesting that there is another, ROCK-independent, pathway that directly recruits NMII to the equatorial cortex. We propose that ROCK and survivin are the two proteins that regulate NMII at the equatorial cortex. Indeed, partial depletion of survivin results in diminishing amounts of NMIIB recruited to the cleavage furrow. Thus, survivin has multiple effects on contractile ring assembly, localization and timing. Survivin–NMIIB colocalization is reduced as mitosis progresses (late telophase and cytokinesis); hence, survivin does not affect NMIIB filament assembly at these stages, and the number of NMIIB molecules in the filament remains constant. Indeed, it has been shown that the number of NMII molecules in contractile rings is roughly constant from the time that a ring condenses through its restriction (Wu and Pollard, 2005).

The importance of survivin–NMIIB interaction is underscored by the findings that any form of disruption of this interaction (i.e. NMIIBΔSBD, survivin^{T34D}, survivin$^{F101A/L102A}$ and survivin$^{L6A/W10A}$) leads to NMIIB over-assembly and mitotic defects. These cells exhibit bipolar, tripolar and multipolar mitosis that ends in cytokinesis failure and furrow regression. NMIIB in these cells over-assembles, forming multiple contractile rings in a random manner, leading to multiple furrows (Fig. 8C). We propose that NMIIB over-assembly leads to the formation of aberrant contractile ring(s) that are unable to divide the cell. It is also likely that the over-assembled NMIIB filaments are unable to disassemble efficiently, a step required for the separation of the daughter cells. Additionally, the random assembly of NMIIB filaments in the midzone and cell cortex may result in contracting forces pulling the daughter cells in different directions, leading to ring regression and furrow regression (Fig. 8C). In sum, Cdk1 indirectly and survivin directly control the contractile ring assembly to ensure that the contractile ring is initiated only after anaphase onset, and that it has the right size and is positioned properly at the precise time. Finally, because the CPC is involved in abscission (Capalbo et al., 2012; Carlton et al., 2012), it is possible that the survivin–NMIIB complex also plays a role in this process.

The dominant-negative effect of the ectopic expression of NMIIBΔSBD may be due to its ability to form contractile-ring-like structures in different places in the cell (Fig. 8C), overcoming the function of endogenous NMIIB that is regulated by survivin. Moreover, because NMIIBΔSBD is capable of co-assembling with endogenous NMIIB (data not shown), it further increases the amounts of NMIIB–NMIIBΔSBD filaments, which may also lead to the formation of multiple contractile-ring-like structures. The dominant-negative effect of the ectopic expression of survivin^{T34D} may be the result of the ability of survivin^{T34D} to interact with the CPC (Barrett et al., 2009), so that survivin^{T34D} competes with the endogenous survivin for the CPC. Furthermore, the ability of survivin^{T34D} to dimerize may lead to the formation of non-functional endogenous survivin–survivin^{T34D} heterodimers.

Whether the homodimerization of survivin is required for survivin functions *in vivo* is unknown. There is evidence that some key protein–protein interactions require a monomeric survivin protein. For example, survivin binds as a monomer to the CPC protein borealin (Bourhis et al., 2007; Jeyaprakash et al., 2007), and cellular localization requires survivin in monomers (Engelsma et al., 2007; Jeyaprakash et al., 2007). We show that disruption of the survivin L6 and W10 dimerization interface leads to the formation of a constitutive monomer, providing experimental proof for the structural data. Furthermore, while disruption of any of the survivin dimerization interfaces (i.e. L6 and W10, or F101 and L102) prevents their binding to NMIIB, these monomeric proteins are capable of binding CPC both *in vivo* and *in vitro*. Thus, survivin in monomers can bind to CPC while only survivin in homodimers interacts with NMIIB, attesting to a functional role for survivin homodimerization.

It is likely that within the cell, survivin resides in two conformations, monomer and homodimer, having different cellular partners and functions. An indication for the existence of survivin in different complexes comes from the findings that a fraction of survivin exists outside the CPC (Bolton et al., 2002; Sasai et al., 2016). We propose that survivin, as a monomer, binds to the CPC to regulate various processes during mitosis, and, as a homodimer, it binds to NMII to regulate cytokinesis. This hypothesis is supported by the findings that survivin$^{L6A/W10A}$ and survivin$^{F101A/L102A}$ have a dominant-negative phenotype.

MATERIALS AND METHODS

Cell lines and culture conditions

HeLa, Cos-7 and HEK293T cell lines were purchased from the American Type Culture Collection (ATCC) and were maintained in high-glucose DMEM (Sigma-Aldrich) supplemented with 2 mM L-glutamine, 10% fetal calf serum (FCS) and antibiotics (100 U/ml penicillin, 100 mg/ml streptomycin and 1:100 Biomyc3 anti-mycoplasma antibiotic solution; Biological Industries, Beit HaEmek, Israel). Cells were grown at 37°C in a humidified atmosphere of 5% CO_2 and 95% air.

Antibodies

Antibodies specific for the C-terminal region of human NMIIB (used at 1:1000 dilution) were generated in rabbits according to the method of Phillips et al. (1995). Recombinant GFP antibodies (used at 1:1000 dilution) were prepared in rabbits as described previously (Rosenberg and Ravid, 2006). Mouse monoclonal β-actin antibodies (A1978, 1:5000) were from Sigma-Aldrich. Rabbit monoclonal survivin antibodies (71G4B7, 1:1000

Journal of Cell Science (2019) 132, jcs233130. doi:10.1242/jcs.233130

for western blot and 1:200 for immunofluorescence) were from Cell Signaling Technology. Mouse monoclonal survivin antibodies (sc-17779, 1:1000.) were from Santa Cruz Biotechnology. Rabbit polyclonal phospho-survivin^{T34} (NB500-236SS, 1:1000 for western blot and 1:200 for immunofluorescence) were from Novus Biologicals. Mouse monoclonal anti-NMIIB (ab684, 1:200), goat polyclonal anti-GFP (ab6673, 1:1000) and rat monoclonal anti-tubulin (ab6160, 1:200) antibodies were from Abcam. Horseradish peroxidase-conjugated secondary antibodies, donkey anti-rat-IgG conjugated to Alexa Fluor 555, goat anti-mouse-IgG conjugated to Alexa Fluor 488, goat anti-rabbit-IgG conjugated to Cy5 and goat anti-mouse conjugated to Cy5 were from Jackson ImmunoResearch Laboratories.

Construction of NMIIB mutants

All primers used for plasmid constructions are presented in Table S1. Restriction enzymes were from New England Biolabs or Fermentas. Rod-BΔACD was created as described previously (Straussman, 2005). To create RodBΔSBD, pET21C-Rod-B (Straussman et al., 2007) was subjected to three-step PCRs. The first and the second PCR was carried out with primers #1 and #4 and primers #2 and #3, respectively (Table S1). The PCR products were subjected to a third PCR reaction using primers #1 and #2. The resulting PCR product was digested with BamHI and EcoRI and ligated into pET21C digested with the same enzymes. For Rod-B^{EtoA} construction, pET21C-Rod-B was subjected to a three-step PCR, the first and the second PCR with primers #1 and #6, and primers #2 and #5, respectively (Table S1). The PCR products were subjected to a third PCR reaction with primers #1 and #2. The resulting PCR product was digested with BamHI and EcoRI and ligated into pET21C digested with the same enzymes. To create GFP–NMIIB mutant constructs, pET21C-Rod-BΔSBD and pET21C-Rod-B^{EtoA} were digested with SmaI and ligated into eGFP-NMIIB-C3 (kindly provided by Dr Robert S. Adelstein, Laboratory of Molecular Cardiology, NIH, USA) digested with SmaI.

Construction of survivin mutants

pcDNA-survivin was kindly provided by Dr Sally Wheatley (University of Nottingham, Nottingham, UK). To create 6×His-tagged survivin (His–survivin), EcoRI and BamHI restriction sites were added to pcDNA-survivin (Ambrosini et al., 1997) by PCR with primers #7 and #8 (Table S1). The PCR product was digested with EcoRI and BamHI and ligated into a pQE80L vector digested with the same enzymes (pQE80L-survivin). The pQE80L-survivin was used as a template in all the cloning reactions described below. To create His–survivin^{T34D}, a three-step PCR was performed, primers #9 and #8, and #10 and #7 (Table S1) were used for the first and second PCR, respectively. The resulting PCR products were subjected to a third PCR reaction with primers #9 and #10. The final PCR product was digested with BamHI and EcoRI and ligated into pQE80L digested with the same enzymes. A similar three-step PCR was used to create His–survivin^{T34A}. The first and second PCR were carried out with primers #9 and #12, and primers #8 and #11, respectively (Table S1). The resulting PCR products were subjected to a third PCR with primers #9 and #10 and the final PCR product was digested with BamHI and EcoRI and ligated into pQE80L digested with the same enzymes. To create His–survivin$^{F101A/L102A}$, the first and second PCR were carried out with primers #9 and #14, and #10 and #13, respectively (Table S1). The resulting PCR products were subjected to a third PCR with primers #9 and #10, and the final PCR product was digested with BamHI and EcoRI and ligated into pQE80L digested with the same enzymes. To create His–survivin$^{L6A/W10A}$, the first and second PCR were carried out with primers #9 and #22, and #10 and #21, respectively (Table S1). The resulting PCR products were subjected to a third PCR with primers #9 and #10 and the final PCR product digested with BamHI and EcoRI and ligated into pQE80L digested with the same enzymes. Cloning of His–survivin^{108} and His–survivin^{118} was undertaken with the Gibson assembly method (Gibson et al., 2009). pQE80L vector was subjected to PCR with primers #15 and #16 (Table S1). To create survivin^{108} and survivin^{118}, primers #17 and #18, and #17 and #19, respectively, were used in the PCRs. The PCR products were digest with DpnI and assembled with Gibson assembly master mix (New England Biolabs) according to the manufacturer's instructions. To clone GFP- or mCherry-tagged survivin proteins, BglII and EcoRI restriction sites were added to pQE80L containing the survivin constructs using primers #8 and #20 (Table S1). The PCR products were digested with BglII and EcoRI and ligated into pEGFP-C1 or pmCherry-C1 digested with the same enzymes. To clone GFP–survivin$^{L6A/W10A}$ or mCherry–survivin$^{F101A/L102A}$, BglII and EcoRI restriction sites were added to pQE80L containing the survivin constructs using primers #23 and #20. The PCR products were digested with BglII and EcoRI and ligated into pEGFP-C1 or pmCherry-C1 digested with the same enzymes. To create the inducible mCherry–survivin expression vector, BmtI and PmeI restriction sites were added by PCR to pmCherry-survivin construct using primers #24 and #25. The PCR products were digested with BmtI and PmeI and ligated into PB-TRE-dCas9-VPR (Chavez et al., 2015) digested with the same enzymes.

Construction of GST–Aurora-B

BamHI and EcoRI restriction sites were added to GFP–Aurora-B (a gift from Dr Susanne M. A. Lens, Department of Medical Oncology, University Medical Center Utrecht, The Netherlands) using primers #26 and #27. The PCR product was digested with BamHI and EcoRI and ligated into pGEX-2T digested with the same enzymes.

Generation of HeLa survivin^{KD} cells

HEK293T cells were seeded on a 10 cm dish. After reaching confluence, cells were transfected with pGag pol, pMPG-VSVG and shScramble (TRC1/1.5, Sigma-Aldrich) or shSurvivin (TRCN0000377600, Sigma-Aldrich) using polyethylenimine (PEI). At 8 h post transfection the medium was replaced with a fresh medium, and at 24, 32 and 36 h post-transfection the supernatant was collected. The supernatant was centrifuged for 30 min at 500 ***g***, filtered with a 0.45 µM filter, aliquoted and stored at −80°C. HeLa cells were infected with the viruses containing the shRNA-Scramble or shRNA-Survivin, and at 24 h post-infection, 2 µg/ml puromycin (Sigma-Aldrich) was added and the cells were grown for additional 72 h. Knockdown of survivin was verified by western blotting.

Generation of the inducible Cos-7 NMIIB^{KD} cell line

To allow conditional knockdown of the NMIIB (*MHY10*) gene, two complementary oligonucleotides were synthesized (Integrated DNA technologies) according to the instructions in Lentiweb.com. These oligonucleotides contained: (1) a sequence targeting the 3′-untranslated region (3'-UTR) of NMIIB mRNA, 5′-CTGCACTTGTCTCTCTCAT-3′; (2) additional sequences to allow a hairpin secondary structure and (3) sequences allowing sticky-end ligation into ClaI and MluI sites. To create double-stranded DNA, 20 µl double-distilled water (DDW), 3 µl (1 mg/ml) of each of the complementary oligonucleotides and 24 µl of 2× annealing buffer (60 mM HEPES-KOH pH 7.4, 200 mM potassium acetate, 4 mM magnesium acetate) were incubated for 4 min at 95°C and then 10 min at 72°C. Then the samples were gradually cooled down to room temperature. 2 µl of hybridization mix were subjected to phosphorylation by 1 µl (10 units) of T4 polynucleotide kinase (Fermentas) in 5 µl DDW and 1 µl of 1 mM ATP for 30 min at 37°C and then at 10 min at 70°C for heat inactivation of the kinase. Phosphorylated hybridized oligonucleotides were subcloned into pLVTHM vector digested with ClaI and MluI. Three 92 mm cell culture dishes with 293T cells at 70–80% confluency were transfected with 10 µg pLVTHM-siNMIIB, 6.5 µg GagPol and 3.5 µg VsvG helper plasmids by using the calcium phosphate method as described previously (Swift et al., 2001). The same amount of cells were transfected with pLV-tTR-KRAB plasmid which expresses the tetracycline repressor of *E. coli* Tn10 fused to the KRAB repression module, along with dsRED protein as an internal marker. The fused protein suppresses the transcription of promoters juxtaposed to the *tet* operator sequence in the pLVTHM plasmid, which includes H1 promoter for siRNA and the EF1 promoter for the mCherry expression marker (Wiznerowicz and Trono, 2003). In our system, addition of doxycycline results in dissociation of tTR-KRAB protein from the *tet* operator allowing expression of siRNA along with the mCherry internal marker. After 16 h incubation, medium from transfected 293T cells was collected and filtrated through a 0.45 µM syringe filter into 36 ml thin-walled tubes (SORVALL, Asheville, NC). After 2 h centrifugation at

113,000 ***g*** 4°C in TST-28 swing-bucket rotor (Kontron Analytical, Redwood City, CA), the supernatant was discarded and the pellet containing the virions was resuspended in a 320 µl total volume of high-glucose DMEM supplemented with 2 mM glutamine and antibiotics plus 10 µg/ml hexadimethrine bromide (Sigma). 310 µl virions from pLVTHM-siNMIIB-transfected cells were combined with 310 µl virions from pLV-tTR-KRAB transfected cells. The growth medium of COS-7 cells was aspirated and cells were incubated with the combined virions mix for 4 h at 37°C. Then, 2 ml complete medium were added to virion mix and cells were grown for additional 24 h at 37°C. Afterwards, the medium was replaced with fresh 2 ml of complete medium. Knockdown of NMIIB was verified by western blotting.

Generation of the HeLa-VPR cell line expressing inducible mCherry–survivin

10^5 HeLa cells were grown on two 35 mm dishes for ∼16 h. Then, cells from one plate were co-transfected with the appropriate VPR–survivin construct and HyperPBase. The cells on the other plate served as a control and were co-transfected with Hyperpbase and GFPpbase (a plasmid without hygromycin resistance) (both were a gift from Dr Maayan Salton, Department of Biochemistry and Molecular Biology, The Hebrew University of Jerusalem, Israel). At ∼16 h post transfection the medium was replaced with fresh medium and the cells were seeded on 60 mm dishes for 16 h. Then, 250 µg/ml hygromycin was added to the VPR-transfected cells as well as to control cells. Once the control cells died, the VPR cells were induced to express mCherry–survivin using 1 µg/ml doxycycline. The expression of mCherry–survivin proteins was detected 16 h after induction.

Protein expression and purification

Rod-B proteins was purified as described previously (Straussman et al., 2007). Survivin proteins were grown in the *E. coli* T7+ strain to an optical density at 600 nm (OD600nm) of 0.5, and 0.5 mM isopropyl-β-D-thiogalactoside (IPTG) was added and the bacteria were grown at 16°C overnight. Bacterial pellets were collected by centrifugation 10,000 ***g*** (Sorvall Thermo-Scientific, Rotor F12) and dissolved in Buffer A containing 50 mM Tris-HCl pH 8, 500 mM NaCl, glycerol 1%, 20 mM imidazole, 20 mM β-mercaptoethanol, 0.5 mM phenylmethylsulfonyl fluoride (PMSF) and 1% Tween-20. Bacteria suspensions were sonicated and centrifuged using F21-8×50y rotor (Thermo-Scientific) at 20,000 ***g*** for 15 min. Supernatants were collected and loaded on a Ni^{2+}-NTA bead column (GE Healthcare) prewashed with Buffer A. The survivin proteins were eluted with Buffer A containing 250 mM imidazole. Fractions containing proteins were pooled and dialyzed against Buffer A without imidazole, and protein concentration was determined with a Nanodrop spectrophotomer. $Survivin^{F101A/L102A}$ was grown in *E. coli* and purified as above except that Buffer A was replaced with a buffer containing 20 mM HEPES pH 8, 500 mM NaCl, 8.7% glycerol, 2.5 mM β-mercaptoethanol and 0.5 mM PMSF (Engelsma et al., 2007). $Survivin^{F101A/L102A}$ and $survivin^{L6A/W10A}$ obtained from the Ni^{2+}-NTA column were further purified by using a HiLoad 16/60 Superdex 75 pg size exclusion chromatography column (GE Healthcare Life Sciences) equilibrated with 20 mM Tris-HCl pH 7.5, 150 mM NaCl and 2 mM DTT. It should be noted that in the experiments using survivin and $survivin^{F101A/L102A}$, both proteins were purified under the same conditions.

GST and GST–Aurora-B were grown in T7+ strain *E. coli* to OD600nm=0.5; then, 0.5 mM IPTG was added and the bacteria were grown for additional 3 h. Bacterial pellets were collected by centrifugation at 10,000 ***g*** (Sorvall, Thermo Scientific, Rotor F12) and resuspended in lysis buffer containing 50 mM Tris-HCl pH 8, 150 mM NaCl, 10 mM EDTA, 1 mM DTT, 10% glycerol and 1 mM PMSF. Bacterial suspensions were sonicated and centrifuged in a F21-8×50y rotor (Thermo Scientific) at 20,000 ***g*** for 15 min. Supernatants were collected and mixed with 500 µl glutathione beads (Rimon Biotech) prewashed with lysis buffer without PMSF. The bacterial lysates and glutathione beads were incubated at 4°C on a rotator for 1–2 h followed by three washes with lysis buffer. GST and GST–Aurora-B coupled to glutathione beads were analyzed on a Coomassie-stained 10% SDS-PAGE gel before being used in the pulldown assay.

Molar mass determination with SEC-MALS

Experiments were performed with a pre-equilibrated analytical SEC column (Superdex 200 10/300 GL; GE Healthcare Life Sciences) with buffer containing 20 mM Tris-HCl pH 8, 2 mM DTT, 100 mM NaCl and 0.01% sodium azide. The accuracy of the system was tested using a protein with a known molecular mass such as BSA. The survivin protein samples (70 µl) were loaded onto an HPLC column connected to an 18-angle light-scattering detector, followed by a differential refractive-index detector (Wyatt Technology). Refractive index and MALS readings were analyzed with the Astra software package (Wyatt Technology) to determine molecular mass.

Direct pulldown assay

Ni^{2+}-NTA beads were equilibrated in Buffer B containing 20 mM Tris-HCl pH 8, 225 mM NaCl, 5% glycerol, 1% NP-40 and 30 mM imidazole. His–survivin proteins (40–45 µg) were added to the beads in a final volume of 200 µl. The beads–survivin protein mix was incubated on a rotator at 4°C for at least 40 min and washed twice with 300 µl Buffer B, incubated for 5 min on rotator at 4°C and the supernatant was removed. Rod-B proteins (40–45 µg) were added to the beads–survivin complex in a final volume of 100 µl. The bead–protein mix was incubated and washed as above and eluted with 30 µl buffer B containing 250 mM imidazole for at least 25 min. The beads were centrifuged for 5 min (>16,000 ***g***) and 25 µl of the supernatant were added to 25 µl SDS sample buffer. For total protein input, 15 µl of the beads–proteins mix were added to 15 µl of SDS sample buffer. Proteins were analyzed on 10–12% SDS-PAGE gels and detected with Coomassie Brilliant Blue.

To test whether monomeric survivin mutants bind to GST–Aurora-B, 10 µg GST or GST–Aurora-B coupled to glutathione beads were incubated with 3 µg survivin proteins in a final volume of 200 µl. The protein–bead mixtures were incubated on rotator at 4°C for 1 h. Then the beads were washed three times with reaction buffer (50 mM Tris-HCl pH 8, 400 mM Nacl, 10 mM EDTA, 1 mM DTT and 10% glycerol). Proteins were analyzed on 12% SDS-PAGE gels and detected with Coomassie Brilliant Blue.

Quantitative *in vitro* binding assay

This assay was performed as described previously (Lapetina and Gil-Henn, 2017) with a few modifications. In brief, Ni^{2+}-NTA beads were equilibrated in Buffer B. Then, different amounts of His–survivin (0–20 µM) were added to the beads in a final volume of 200 µl. The beads–survivin protein mix was incubated on a rotator at 4°C for at least 40 min and were quickly washed twice with 200 µl Buffer B. 0.5 µM recombinant Rod-B was added to each beads-survivin complex in a final volume of 200 µl. The bead–survivin–Rod-B mix was incubated and washed as above. After the second wash, the beads were dried, and 30 µl SDS-sample buffer was added. The whole sample was loaded on a 10% SDS-PAGE and detected with Coomassie Briliant Blue. For measurements of dissociation constant (K_d), band densities were quantified using imageJ and binding isotherms were set using Prism (GraphPad Software) with the one site-specific binding equation: $Y=B_{max}\times X/X+K_d$. In this equation, Y equals the specific binding signal, X equals the concentration of survivin, and B_{max} is the maximum specific binding. The dissociation constant K_d is solved as the value of X when Y equals 50% of B_{max}. To ensure saturation of the curves, survivin maximal concentrations of at least five times the K_d were used in the assay.

Co-immunoprecipitation assay

1×10^6–2×10^6 HeLa or HEK293T cells were seeded on a 60 mm dish. After attaching to the dish (10–24 h), cells were transfected with 6 µg DNA per plate, mixed with 36 µg Linear PEI (L.PEI). Cells were harvested at 24–48 h post transfection with 300 µl extraction buffer [20 mM Tris-HCl pH 8.0, 225 mM NaCl, 0.5 mM EDTA, 1% NP-40, 1 mM DTT and protease inhibitor cocktail (Sigma-Aldrich)]. Cell extracts were sonicated and centrifuged in 4°C for at least 15 min (>16,000 ***g***). Anti-NMIIB antibodies were incubated with protein A/G beads (Santa Cruz Biotechnology) prewashed with 300 µl extraction buffer on a rotator at

4°C for 1.5–2 h. The beads–antibodies mix was washed three times with extraction buffer. The cell extracts were added to the bead–antibody mix and were incubated for 1.5–2 h on rotator at 4°C. Then, the mix was washed three times in extraction buffer and analyzed by western blotting using antibodies for NMIIB and GFP. The co-immunoprecipitation assay using Cos-7-NMIIB^{KD} cells was carried out as above except that the cells were treated with 0.2 µg/ml doxycycline (Sigma-Aldrich) for 24 h before transfected with 1.2 µg HA–survivin and 4.8 µg GFP–NMIIB constructs. At 48 h post transfection, cells were harvested and subjected to co-immunoprecipitation assay with anti-GFP antibody. For total protein analysis, 30 µl of the cell extracts were added to 7.5 µl SDS sample buffer. For endogenous survivin and NMIIB co-immunoprecipitation, 6×10^8 cells were seeded. Before harvesting, 10 µM RO-3306 (Sigma-Aldrich) was added for 1 h. Cells were harvested with extraction buffer containing 5% glycerol. Cells were sonicated and the co-immunoprecipitation assay was carried out as above.

Co-immunoprecipitation of mCherry–survivin and endogenous NMIIB using HeLa-VPR mCherry-survivin cells was undertaken as follows. At 24 h prior to the experiment, 1 µg/ml doxycycline was added to the cells and, after 8–10 h, 10 µM S-trityl-L-cysteine (STLC) (Sigma-Aldrich) was added. The mitotic cells were collected by mitotic shake-off in a medium containing STLC. 3×10^6 cells were seeded on two 35 mm plates coated with poly-D-lysine (PDL) and allowed to attach for 20–30 min. Cells from one plate were lysed right after the attachment, whereas the other plate was released into fresh medium without STLC for 3 h before cell lysis. The co-immunoprecipitation assay was carried out as above.

Immunofluorescence and live imaging

Cells were treated with 10 µM STLC for 12–16 h. Then cells were harvested by mitotic shake-off and 3×10^5–4×10^5 cells were seeded on PDL-coated coverslips. After attachment (~10–15 min after seeding), the medium was replaced with fresh medium and cells were incubated for 2.5 h, fixed with 4% formaldehyde in PBS, washed three times with PBS and permeabilized for 3 min with PBS containing 0.2% Triton X-100 and 0.5% BSA. After three washes with PBS, cells were blocked with horse serum diluted 1:50 for 35 min at 37°C. Cells were washed, and primary antibodies in PBS containing 0.1% BSA were added and incubated for 2 h at 37°C or overnight at 4°C. Coverslips were washed three times with PBS, and secondary antibodies were added and incubated for 1 h at 37°C. Where indicated, 300 nM DAPI (Sigma-Aldrich) was added to the coverslips and incubated for 5 min at room temperature. Coverslips were mounted on slides (Thermo Scientific) using Vectachield mounting medium (Vector Laboratories Inc.). Confocal images were obtained with a Zeiss LSM 710 Axio Observer.Z1 microscope with a 63×/1.4 oil DIC M27 or Nikon A1R with 1.4 CFI plan Apo Lambda 60× oil objective. Optical sections were collected at 500 nm interval. Images analysis and 3D reconstitution were carried out using NIS-Elements AR.

For live imaging, 1×10^6–2×10^6 HeLa cells were seeded onto a 60 mm dish for 12–16 h, and then cells were transfected with the appropriate constructs (1.2 µg mCherry–survivin and 4.8 µg GFP–NMIIB). At 36 h post transfection, STLC was added for 12–16 h. Then 4×10^5 cells were seeded in a PDL-coated chamber (Ibidi); after attachment the medium was replaced with a fresh medium and after 1–1.5 h live cell imaging was carried out at 37°C and 5% CO_2. Live images were taken every 3–15 min using a Nikon Ti microscope with a Plan-Apochromat 63×/1.40 oil DIC M27 objective. Exposure times for GFP–NMIIB and mCherry–survivin were 100 ms and 40 ms, respectively.

Fluorescence quantification

Line scans of endogenous survivin and NMIIB were generated along the division plane using the ImageJ software package (National Institutes of Health, Bethesda, MD). To determine the percentage of survivin and NMIIB in the cleavage furrow, the fluorescence intensity of each protein in the cleavage furrow and in the entire cell was determined with ImageJ software and according to previous guidelines (Lee and Kitaoka, 2018). Then, the protein intensity in the cleavage furrow was divided by its intensity in the entire cell. Background fluorescence was measured outside the cell, and this value was subtracted from all the intensity measurements.

To determine the phospho-survivin^{T34} levels, the fluorescence intensity of the anti-phospho-survivin^{T34} antibodies signal was quantified using ImageJ software. Background fluorescence was measured outside the cell and was subtracted from the phospho-survivin^{T34} signal.

For colocalization analysis, the Pearson correlation coefficient (PCC) was calculated between the intensity profiles of NMIIB and survivin along the cell cortex (for metaphase) and along the cleavage furrow (for anaphase and telophase) as indicated in Fig. S1B. The PCC was calculated using Excel (Microsoft) and Prism 6 (GraphPad). Statistical analysis was done using Prism 6. Data were examined by one-way ANOVA for variances, followed by a two-tailed Student's *t*-test between each group.

Rod-B solubility assay

The solubility assay was performed as described (Dahan et al., 2014). Briefly, Rod-B (8.5 µg/120 µl) was dialyzed against Buffer G (10 mM phosphate buffer pH 7.5, 2 mM $MgCl_2$, 1 mM DTT and 200 mM NaCl) for 4–16 h at 4°C. Then 100 µl of Rod-B was centrifuged at high speed (135,000 ***g***) using Beckman-Coulter centrifuge tubes. 80 µl from the supernatant (non-filamentous NMII) was added to a fresh tube containing 20 µl 5× SDS sample buffer. 100 µl Buffer G was added to the pellet (filamentous NMII) and the tubes were vortexed at 900 rpm for 30 min. Then 25 µl 5× SDS sample buffer was added to the pellet. When indicated, 4 µg survivin added to Rod-B before dialysis. Samples were analyzed on 10% SDS-PAGE gels stained with Coomassie Brilliant Blue, scanned and quantified using the densitometry program ImageGauge V (Fujifilm, Tokyo, Japan).

Acknowledgements

We thank Dario C. Altieri and Sally P. Wheatley for providing survivin constructs, and Robert S. Adelstein for NMII constructs; Yael Feinstein Rotkopf and Zakhariya Manevitch for technical assistance with the microscopy work. S.R. holds the Dr Daniel G. Miller Chair in Cancer Research.

Competing interests

The authors declare no competing or financial interests.

Author contributions

Conceptualization: A.B., D.R., S.R.; Methodology: A.B., M.R., R.W., S.R.; Validation: A.B., E.C., H.A.; Formal analysis: A.B.; Investigation: A.B., E.C., H.A., D.R., M.R.; Resources: A.B.; Writing - original draft: A.B., S.R.; Writing - review & editing: A.B.; Visualization: A.B., S.R.; Supervision: S.R.

Funding

This research received no specific grant from any funding agency in the public, commercial or not-for-profit sectors funding section.

Supplementary information

Supplementary information available online at
http://jcs.biologists.org/lookup/doi/10.1242/jcs.233130.supplemental

References

Aljaberi, A. M., Webster, J. R. M. and Wheatley, S. P. (2015). Mitotic activity of survivin is regulated by acetylation at K129. *Cell Cycle* **14**, 1738-1747. doi:10.1080/15384101.2015.1033597

Ambrosini, G., Adida, C. and Altieri, D. C. (1997). A novel anti-apoptosis gene, survivin, expressed in cancer and lymphoma. *Nat. Med.* **3**, 917-921. doi:10.1038/nm0897-917

Bao, J., Jana, S. S. and Adelstein, R. S. (2005). Vertebrate nonmuscle myosin II isoforms rescue small interfering RNA-induced defects in COS-7 cell cytokinesis. *J. Biol. Chem.* **280**, 19594-19599. doi:10.1074/jbc.M501573200

Barrett, R. M. A., Colnaghi, R. and Wheatley, S. P. (2011). Threonine 48 in the BIR domain of survivin is critical to its mitotic and anti-apoptotic activities and can be phosphorylated by CK2 in vitro. *Cell Cycle* **10**, 538-548. doi:10.4161/cc.10.3.14758

Barrett, R. M. A., Osborne, T. P. and Wheatley, S. P. (2009). Phosphorylation of survivin at threonine 34 inhibits its mitotic function and enhances its cytoprotective activity. *Cell Cycle* **8**, 278-283. doi:10.4161/cc.8.2.7587

Beach, J. R. and Egelhoff, T. T. (2009). Myosin II recruitment during cytokinesis independent of centralspindlin-mediated phosphorylation. *J. Biol. Chem.* **284**, 27377-27383. doi:10.1074/jbc.M109.028316

Bement, W. M., Benink, H. A. and von Dassow, G. (2005). A microtubule-dependent zone of active RhoA during cleavage plane specification. *J. Cell Biol.* **170**, 91-101. doi:10.1083/jcb.200501131
Bolton, M. A., Lan, W., Powers, S. E., McCleland, M. L., Kuang, J. and Stukenberg, P. T. (2002). Aurora B kinase exists in a complex with survivin and INCENP and its kinase activity is stimulated by survivin binding and phosphorylation. *Mol. Biol. Cell* **13**, 3064-3077. doi:10.1091/mbc.e02-02-0092
Bourhis, E., Hymowitz, S. G. and Cochran, A. G. (2007). The mitotic regulator Survivin binds as a monomer to its functional interactor Borealin. *J. Biol. Chem.* **282**, 35018-35023. doi:10.1074/jbc.M706233200
Capalbo, L., Montembault, E., Takeda, T., Bassi, Z. I., Glover, D. M. and D'Avino, P. P. (2012). The chromosomal passenger complex controls the function of endosomal sorting complex required for transport-III Snf7 proteins during cytokinesis. *Open Biol.* **2**, 120070. doi:10.1098/rsob.120070
Carlton, J. G., Caballe, A., Agromayor, M., Kloc, M. and Martin-Serrano, J. (2012). ESCRT-III governs the Aurora B-mediated abscission checkpoint through CHMP4C. *Science* **336**, 220-225. doi:10.1126/science.1217180
Carmena, M., Wheelock, M., Funabiki, H. and Earnshaw, W. C. (2012). The chromosomal passenger complex (CPC): from easy rider to the godfather of mitosis. *Nat. Rev. Mol. Cell Biol.* **13**, 789-803. doi:10.1038/nrm3474
Carvalho, A., Carmena, M., Sambade, C., Earnshaw, W. C. and Wheatley, S. P. (2003). Survivin is required for stable checkpoint activation in taxol-treated HeLa cells. *J. Cell Sci.* **116**, 2987-2998. doi:10.1242/jcs.00612
Chang, D. C., Xu, N. and Luo, K. Q. (2003). Degradation of cyclin B is required for the onset of anaphase in Mammalian cells. *J. Biol. Chem.* **278**, 37865-37873. doi:10.1074/jbc.M306376200
Chantalat, L., Skoufias, D. A., Kleman, J.-P., Jung, B., Dideberg, O. and Margolis, R. L. (2000). Crystal structure of human survivin reveals a bow tie-shaped dimer with two unusual alpha-helical extensions. *Mol. Cell* **6**, 183-189. doi:10.1016/S1097-2765(05)00020-1
Chavez, A., Scheiman, J., Vora, S., Pruitt, B. W., Tuttle, M., P R Iyer, E., Lin, S., Kiani, S., Guzman, C. D., Wiegand, D. J. et al. (2015). Highly efficient Cas9-mediated transcriptional programming. *Nat. Methods* **12**, 326-328. doi:10.1038/nmeth.3312
Cohen, C. and Parry, D. A. (1998). A conserved C-terminal assembly region in paramyosin and myosin rods. *J. Struct. Biol.* **122**, 180-187. doi:10.1006/jsbi.1998.3983
Colnaghi, R. and Wheatley, S. P. (2010). Liaisons between survivin and Plk1 during cell division and cell death. *J. Biol. Chem.* **285**, 22592-22604. doi:10.1074/jbc.M109.065003
Dahan, I., Yearim, A., Touboul, Y. and Ravid, S. (2012). The tumor suppressor Lgl1 regulates NMII-A cellular distribution and focal adhesion morphology to optimize cell migration. *Mol. Biol. Cell* **23**, 591-601. doi:10.1091/mbc.e11-01-0015
Dahan, I., Petrov, D., Cohen-Kfir, E. and Ravid, S. (2014). The tumor suppressor Lgl1 forms discrete complexes with NMII-A and Par6alpha-aPKCzeta that are affected by Lgl1 phosphorylation. *J. Cell Sci.* **127**, 295-304. doi:10.1242/jcs.127357
D'Avino, P. P., Giansanti, M. G. and Petronczki, M. (2015). Cytokinesis in animal cells. *Cold Spring Harb. Perspect Biol.* **7**, a015834. doi:10.1101/cshperspect.a015834
Dean, S. O. and Spudich, J. A. (2006). Rho kinase's role in myosin recruitment to the equatorial cortex of mitotic Drosophila S2 cells is for myosin regulatory light chain phosphorylation. *PLoS ONE* **1**, e131. doi:10.1371/journal.pone.0000131
Dulyaninova, N. G., Malashkevich, V. N., Almo, S. C. and Bresnick, A. R. (2005). Regulation of myosin-IIA assembly and Mts1 binding by heavy chain phosphorylation. *Biochemistry* **44**, 6867-6876. doi:10.1021/bi0500776
Engelsma, D., Rodriguez, J. A., Fish, A., Giaccone, G. and Fornerod, M. (2007). Homodimerization antagonizes nuclear export of survivin. *Traffic* **8**, 1495-1502. doi:10.1111/j.1600-0854.2007.00629.x
Gibson, D. G., Young, L., Chuang, R.-Y., Venter, J. C., Hutchison, C. A., III and Smith, H. O. (2009). Enzymatic assembly of DNA molecules up to several hundred kilobases. *Nat. Methods* **6**, 343-345. doi:10.1038/nmeth.1318
Hill, E., Clarke, M. and Barr, F. A. (2000). The Rab6-binding kinesin, Rab6-KIFL, is required for cytokinesis. *EMBO J.* **19**, 5711-5719. doi:10.1093/emboj/19.21.5711
Honda, R., Körner, R. and Nigg, E. A. (2003). Exploring the functional interactions between Aurora B, INCENP, and survivin in mitosis. *Mol. Biol. Cell* **14**, 3325-3341. doi:10.1091/mbc.e02-11-0769
Huxley, A. F. (1957). Muscle structure and theories of contraction. *Prog. Biophys. Biophys. Chem.* **7**, 225-318. doi:10.1016/S0096-4174(18)30128-8
Jeyaprakash, A. A., Klein, U. R., Lindner, D., Ebert, J., Nigg, E. A. and Conti, E. (2007). Structure of a Survivin-Borealin-INCENP core complex reveals how chromosomal passengers travel together. *Cell* **131**, 271-285. doi:10.1016/j.cell.2007.07.045
Kelly, A. E., Ghenoiu, C., Xue, J. Z., Zierhut, C., Kimura, H. and Funabiki, H. (2010). Survivin reads phosphorylated histone H3 threonine 3 to activate the mitotic kinase Aurora B. *Science* **330**, 235-239. doi:10.1126/science.1189505
Kitagawa, M., Fung, S. Y. S., Onishi, N., Saya, H. and Lee, S. H. (2013). Targeting Aurora B to the equatorial cortex by MKlp2 is required for cytokinesis. *PLoS ONE* **8**, e64826. doi:10.1371/journal.pone.0064826
Lapetina, S. and Gil-Henn, H. (2017). A guide to simple, direct, and quantitative in vitro binding assays. *J. Biol. Method.* **4**, e62. doi:10.14440/jbm.2017.161
Lee, J.-Y. and Kitaoka, M. (2018). A beginner's guide to rigor and reproducibility in fluorescence imaging experiments. *Mol. Biol. Cell* **29**, 1519-1525. doi:10.1091/mbc.E17-05-0276
Li, Z.-H., Spektor, A., Varlamova, O. and Bresnick, A. R. (2003). Mts1 regulates the assembly of nonmuscle myosin-IIA. *Biochemistry* **42**, 14258-14266. doi:10.1021/bi0354379
Lister, I. M. B., Tolliday, N. J. and Li, R. (2006). Characterization of the minimum domain required for targeting budding yeast myosin II to the site of cell division. *BMC Biol.* **4**, 19. doi:10.1186/1741-7007-4-19
Matsumura, F., Yamakita, Y. and Yamashiro, S. (2011). Myosin light chain kinases and phosphatase in mitosis and cytokinesis. *Arch. Biochem. Biophys.* **510**, 76-82. doi:10.1016/j.abb.2011.03.002
Maupin, P., Phillips, C. L., Adelstein, R. S. and Pollard, T. D. (1994). Differential localization of myosin-II isozymes in human cultured cells and blood cells. *J. Cell Sci.* **107**, 3077-3090.
Motegi, F., Mishra, M., Balasubramanian, M. K. and Mabuchi, I. (2004). Myosin-II reorganization during mitosis is controlled temporally by its dephosphorylation and spatially by Mid1 in fission yeast. *J. Cell Biol.* **165**, 685-695. doi:10.1083/jcb.200402097
Murakami, N., Kotula, L. and Hwang, Y.-W. (2000). Two distinct mechanisms for regulation of nonmuscle myosin assembly via the heavy chain: phosphorylation for MIIB and mts 1 binding for MIIA. *Biochemistry* **39**, 11441-11451. doi:10.1021/bi000347e
Nishimura, Y. and Yonemura, S. (2006). Centralspindlin regulates ECT2 and RhoA accumulation at the equatorial cortex during cytokinesis. *J. Cell Sci.* **119**, 104-114. doi:10.1242/jcs.02737
Nurse, P. (1990). Universal control mechanism regulating onset of M-phase. *Nature* **344**, 503-508. doi:10.1038/344503a0
O'Connor, D. S., Grossman, D., Plescia, J., Li, F., Zhang, H., Villa, A., Tognin, S., Marchisio, P. C. and Altieri, D. C. (2000). Regulation of apoptosis at cell division by p34cdc2 phosphorylation of survivin. *Proc. Natl. Acad. Sci. USA* **97**, 13103-13107. doi:10.1073/pnas.240390697
Pavlyukov, M. S., Antipova, N. V., Balashova, M. V., Vinogradova, T. V., Kopantzev, E. P. and Shakhparonov, M. I. (2011). Survivin monomer plays an essential role in apoptosis regulation. *J. Biol. Chem.* **286**, 23296-23307. doi:10.1074/jbc.M111.237586
Phillips, C. L., Yamakawa, K. and Adelstein, R. S. (1995). Cloning of the cDNA encoding human nonmuscle myosin heavy chain-B and analysis of human tissues with isoform-specific antibodies. *J. Muscle Res. Cell Motil.* **16**, 379-389. doi:10.1007/BF00114503
Robinson, D. N., Cavet, G., Warrick, H. M. and Spudich, J. A. (2002). Quantitation of the distribution and flux of myosin-II during cytokinesis. *BMC Cell Biol.* **3**, 4. doi:10.1186/1471-2121-3-4
Ronen, D. and Ravid, S. (2009). Myosin II tailpiece determines its paracrystal structure, filament assembly properties, and cellular localization. *J. Biol. Chem.* **284**, 24948-24957. doi:10.1074/jbc.M109.023754
Rosenberg, M. and Ravid, S. (2006). Protein kinase Cgamma regulates myosin IIB phosphorylation, cellular localization, and filament assembly. *Mol. Biol. Cell* **17**, 1364-1374. doi:10.1091/mbc.e05-07-0597
Sabry, J. H., Moores, S. L., Ryan, S., Zang, J.-H. and Spudich, J. A. (1997). Myosin heavy chain phosphorylation sites regulate myosin localization during cytokinesis in live cells. *Mol. Biol. Cell* **8**, 2605-2615. doi:10.1091/mbc.8.12.2605
Sasai, K., Katayama, H., Hawke, D. H. and Sen, S. (2016). Aurora-C interactions with survivin and INCENP reveal shared and distinct features compared with aurora-B chromosome passenger protein complex. *PLoS ONE* **11**, e0157305. doi:10.1371/journal.pone.0157305
Sohn, R. L., Vikstrom, K. L., Strauss, M., Cohen, C., Szent-Gyorgyi, A. G. and Leinwand, L. A. (1997). A 29 residue region of the sarcomeric myosin rod is necessary for filament formation. *J. Mol. Biol.* **266**, 317-330. doi:10.1006/jmbi.1996.0790
Straussman, R. (2005). New insights into the assembly properties of myosin II. *PhD thesis.* The Hebrew University of Jerusalem, Israel.
Straussman, R., Ben-Ya'acov, A., Woolfson, D. N. and Ravid, S. (2007). Kinking the coiled coil-negatively charged residues at the coiled-coil interface. *J. Mol. Biol.* **366**, 1232-1242. doi:10.1016/j.jmb.2006.11.083
Sun, C., Nettesheim, D., Liu, Z. and Olejniczak, E. T. (2005). Solution structure of human survivin and its binding interface with Smac/Diablo. *Biochemistry* **44**, 11-17. doi:10.1021/bi0485171
Swift, S., Lorens, J., Achacoso, P. and Nolan, G. P. (2001). Rapid production of retroviruses for efficient gene delivery to mammalian cells using 293T cell-based systems. *Curr. Protoc. Immunol.* Chapter 10, Unit 10 17C. doi:10.1002/0471142735.im1017cs31
Vader, G., Kauw, J. J. W., Medema, R. H. and Lens, S. M. (2006). Survivin mediates targeting of the chromosomal passenger complex to the centromere and midbody. *EMBO Rep.* **7**, 85-92. doi:10.1038/sj.embor.7400562

Vale, R. D., Spudich, J. A. and Griffis, E. R. (2009). Dynamics of myosin, microtubules, and Kinesin-6 at the cortex during cytokinesis in Drosophila S2 cells. *J. Cell Biol.* **186**, 727-738. doi:10.1083/jcb.200902083

Verdecia, M. A., Huang, H., Dutil, E., Kaiser, D. A., Hunter, T. and Noel, J. P. (2000). Structure of the human anti-apoptotic protein survivin reveals a dimeric arrangement. *Nat. Struct. Biol.* **7**, 602-608. doi:10.1038/77929

Vicente-Manzanares, M., Ma, X., Adelstein, R. S. and Horwitz, A. R. (2009). Non-muscle myosin II takes centre stage in cell adhesion and migration. *Nat. Rev. Mol. Cell Biol.* **10**, 778-790. doi:10.1038/nrm2786

Wang, F., Dai, J., Daum, J. R., Niedzialkowska, E., Banerjee, B., Stukenberg, P. T., Gorbsky, G. J. and Higgins, J. M. G. (2010). Histone H3 Thr-3 phosphorylation by Haspin positions Aurora B at centromeres in mitosis. *Science* **330**, 231-235. doi:10.1126/science.1189435

Wheatley, S. P., Henzing, A. J., Dodson, H., Khaled, W. and Earnshaw, W. C. (2004). Aurora-B phosphorylation in vitro identifies a residue of survivin that is essential for its localization and binding to inner centromere protein (INCENP) in vivo. *J. Biol. Chem.* **279**, 5655-5660. doi:10.1074/jbc.M311299200

Wheatley, S. P., Barrett, R. M., Andrews, P. D., Medema, R. H., Morley, S. J., Swedlow, J. R. and Lens, S. M. A. (2007). Phosphorylation by aurora-B negatively regulates survivin function during mitosis. *Cell Cycle* **6**, 1220-1230. doi:10.4161/cc.6.10.4179

Wieser, S. and Pines, J. (2015). The biochemistry of mitosis. *Cold Spring Harb. Perspect Biol.* **7**, a015776. doi:10.1101/cshperspect.a015776

Wiznerowicz, M. and Trono, D. (2003). Conditional suppression of cellular genes: lentivirus vector-mediated drug-inducible RNA interference. *J. Virol.* **77**, 8957-8961. doi:10.1128/JVI.77.16.8957-8951.2003

Wu, J.-Q. and Pollard, T. D. (2005). Counting cytokinesis proteins globally and locally in fission yeast. *Science* **310**, 310-314. doi:10.1126/science.1113230

Yamagishi, Y., Honda, T., Tanno, Y. and Watanabe, Y. (2010). Two histone marks establish the inner centromere and chromosome bi-orientation. *Science* **330**, 239-243. doi:10.1126/science.1194498

Yang, D., Welm, A. and Bishop, J. M. (2004). Cell division and cell survival in the absence of survivin. *Proc. Natl. Acad. Sci. USA* **101**, 15100-15105. doi:10.1073/pnas.0406665101

Yüce, O., Piekny, A. and Glotzer, M. (2005). An ECT2-centralspindlin complex regulates the localization and function of RhoA. *J. Cell Biol.* **170**, 571-582. doi:10.1083/jcb.200501097

Zhou, M. and Wang, Y.-L. (2008). Distinct pathways for the early recruitment of myosin II and actin to the cytokinetic furrow. *Mol. Biol. Cell* **19**, 318-326. doi:10.1091/mbc.e07-08-0783